Fenoglio-Marc, L.; Rietbroek, R.; Grayek, S.; Becker, M.;
Kusche, J.; Stanev, E.:

Water mass variation in the Mediterranean and Black Seas

In: Journal of Geodynamics (2012) Elsevier

DOI: 10.1016/j.jog.2012.04.001

Water mass variation in the Mediterranean and Black Sea

L. Fenoglio-Marc[a], R. Rietbroek[b], S. Grayek[c], M. Becker[a], J. Kusche[b], E. Stanev[c,d]

[a]*Institute of Physical Geodesy, Technical University Darmstadt*
[b]*Institute of Geodesy and Geoinformation, Bonn University*
[c]*Institut für Chemie und Biologie des Meeres, Oldenburg University*
[d]*Institute for Coastal Research, Helmholtz Zentrum Geesthacht*

Abstract

The mass-induced sea level variability and the net mass transport between Mediterranean Sea and Black Sea are derived for the interval between August 2002 and July 2008 from satellite-based observations and from model data. We construct in each basin two time series representing the basin mean mass signal in terms of equivalent water height. The first series is obtained from steric-corrected altimetry while the other is deduced from GRACE data corrected for the contamination by continental hydrology. The series show a good agreement in terms of annual and inter-annual signals, which is in line with earlier works, although different model corrections influence the consistency in terms of seasonal signal and trend.

In the Mediterranean Sea, we obtain the best agreement using a steric correction from the regional oceanographic model MFSTEP and a continental hydrological leakage correction derived from the global continental hydrology model WaterGAP2. The inter-annual time series show a correlation of

Email address: fenoglio@ipg.tu-darmstadt.de (L. Fenoglio-Marc)

0.85 and a root mean square difference (RMS) of 15 mm. The two estimates have similar accuracy and their annual amplitude and phase agree within 3 mm and 23 days respectively. The GRACE-derived mass-induced sea level variability yields an annual amplitude of 27±5 mm peaking in December and a trend of 5.3±1.9 $^{\mathrm{mm}}/_{\mathrm{yr}}$, which deviates within 3 $^{\mathrm{mm}}/_{\mathrm{yr}}$ from the altimetry-derived estimate.

In the Black Sea, the series are less consistent, with lower accuracy of the GRACE-derived estimate, but still show a promising agreement considering the smaller size of the basin. The best agreement is realized choosing the corrections from WaterGAP2 and from the regional oceanographic model NEMO. The inter-annual time series have a correlation and RMS differences of 0.68 and 55 mm, their annual amplitude and phase agree within 4 mm and 6 days respectively. The GRACE-derived seawater mass signal has an annual amplitude of 32±4 mm peaking in April. On inter-annual time scales, the mass-induced sea level variability is stronger than in the Mediterranean Sea, with an increase from 2003 to 2005 followed by a decrease from 2006 to 2008.

Based on mass conservation, the mass-induced sea level variations, river runoff and precipitation minus evaporation are combined to derive the strait flows between the basins and with the Atlantic Ocean. At the Gibraltar strait, the net inflow varies annually with an amplitude of $52\pm10\times\ 10^{-3}$ Sv peaking end of September (1 Sv = $10^6 m^3 s^{-1}$). The inflow through the Bosphorus strait displays an annual amplitude of $13\pm3\times10^{-3}$ Sv peaking in the middle of March. Additionally, an increase of the Gibraltar net inflow ($3.4\pm0.8\times10^{-3}$ $^{\mathrm{Sv}}/_{\mathrm{yr}}$) is detected.

Keywords: GRACE, sea level, mass change, Mediterranean Sea, Black Sea

1. Introduction

Being an almost closed sub-system, the Mediterranean-Black Sea region provides an interesting setting to study regional mass transports and redistribution.

The two semi-enclosed seas and the Atlantic Ocean are connected by the Bosphorus Strait and by the Gibraltar Strait respectively. Considering its size, the Mediterranean Sea is five times larger than the Black Sea ($2.5 \times 10^{12}\,\mathrm{m}^2$ versus $0.42 \times 10^{12}\,\mathrm{m}^2$). The Mediterranean Sea can be classified as a lagoon-type basin, whereas the Black Sea is an estuarine-type basin. Although the region is densely populated, many components of the water cycle are still poorly quantified. For example, for the river-runoff R and the strait flows of Gibraltar (FG) and Bosphorus (FB) only climatological estimates are available (Mariotti et al. (2002), Grayek et al. (2010)) .

Starting from 2002, the Gravity Recovery and Climate Experiment (GRACE) mission has been providing observations of water mass change, by measuring small variations of the Earth's gravity field that predominantly originate from mass redistributions in the Earth's system (Tapley et al. (2004)). Generally, in order to cope with increasing noise and artefacts present in the high resolution components of the GRACE models, the GRACE models are smoothed by convolution with a kernel of gradually decreasing power. Isotropic (Wahr et al. (1998)) and non-isotropic (Han et al. (2005)) smoothing as well as empirical de-correlation (Swenson and Wahr (2006)) and regularization (Kusche

(2007), Kusche et al. (2009)) have been applied. The smoothing procedure reduces the correlated noise at the cost of signal attenuation and a decreased spatial resolution.

For basin averages, these side effects depend on (1) the type of the signal, (2) the smoothing applied and (3) the dimension and shape of the region (Klees et al. (2007), Kusche (2007)). In regional studies on small ocean basins, filtering causes significant leakage of terrestrial hydrology in the oceanic mass estimated from GRACE, as the land signal is typically much larger. Retrieval of GRACE derived ocean mass variations in small ocean basins presents additional difficulties, as the dimension of the regions are small compared to the resolution of filtered GRACE estimates (Chambers (2006)). Furthermore, the oceanic background models used for de-aliasing the measurements have marginal performance in semi-enclosed basins, which increases the noise in the estimated GRACE residuals (Flechtner (2007a,b)).

Alternatively, steric-corrected altimetry also observes water mass changes. The satellite radar altimetry provides total (steric plus non-steric) sea level heights with an accuracy close to 3 cm (Beckley et al. (2007)). In order to correct the total sea level for its steric component, this last is derived from either observed or modelled temperature and salinity. Several studies have compared steric corrected altimetry with estimates from GRACE at both global (Chambers (2006), Leuliette and Miller (2009), Willis et al. (2008)) and regional scales (Swenson and Wahr (2007), Fenoglio-Marc et al. (2006, 2007), Garcia et al. (2006, 2010), Calafat et al. (2010)) and have shown that

the two methods yield mass change estimates which are consistent at both seasonal and inter-annual time-scales. This paper is an extension of our previous analysis in the Mediterranean Sea (Fenoglio-Marc et al. (2006, 2007)) to a larger region including the Black Sea.

The main objectives of this paper are to assess in semi-enclosed basins the ability of GRACE to recover (1) the seawater mass variations at both seasonal and inter-annual time-scales and (2) the total water budget and its various components. The effect of filtering the basin averages as well as the magnitude and consistency of the corrections applied are investigated.

2. Methodology

2.1. GRACE gravimetry

We use global GRACE gravity field monthly solutions (GSM) provided by the GeoForschungsZentrum (GFZ) (level-2 products, release 4) between August 2002 and July 2008, which contain atmosphere- and ocean-corrected gravity field solutions expressed in Stokes coefficients from degree 2 to degree 120. Since we consider the complete oceanographic signal, we restore the background models, subtracted at an earlier stage during the GRACE processing. We restore here the signal over the ocean areas using the GRACE GAD product, which contains monthly averaged values of the Ocean Model for Circulation and Tides (OMCT) and of the atmospheric model of the European Centre for the Medium Range Weather Forecasts (ECMWF)(Flechtner (2007a)). To enable a comparison with altimetry, we subtract the oceanic averages of the atmospheric pressure, according to Willis et al. (2008). This

ensures that the atmospheric contribution in GRACE is consistent with the inverse barometer (IB) correction which is applied to altimetry.

The GRACE J_2 coefficient is less accurate than the estimates from satellite laser ranging (SLR) (Cheng and Tapley (2004)). Additionally, GRACE does not observe geocenter variation, which is reflected in the degree 1 coefficients. We therefore replace the J_2 coefficient with one obtained from SLR (Cheng and Tapley (2004)) and apply a correction accounting for the annual and semi-annual geocenter motion derived from a joint GRACE, GPS and Ocean Bottom Pressure (OBP) loading inversion (Rietbroek et al. (2009), Rietbroek et al. (2011) this issue). This latter correction, expressed in equivalent water heights, accounts in our region for up to 20 mm.

The error structure of the GRACE solutions is characterized by an increase in errors for coefficients of higher degrees. Furthermore, due to the observation geometry, strong non-physical north-south features are present in the standard solutions (Kusche et al. (2009)). We therefore apply a post-processing/smoothing to the GRACE fields. We calculate a smoothed basin average in terms of equivalent water heights as follows (Swenson and Wahr (2002)):

$$\widetilde{S}^{g}_{rsl}(t) = A_{\tilde{\vartheta}} \frac{a\rho_e}{3\rho_w \vartheta_{00}} \sum_{l=1}^{lmax} \sum_{m=0}^{l} \frac{2l+1}{1+k_l} \{\tilde{\vartheta}^{C}_{lm} \Delta C^{G}_{lm}(t) + \tilde{\vartheta}^{S}_{lm} \Delta S^{G}_{lm}(t)\} \qquad (1)$$

where the 4π-normalized coefficients, ΔC^{G}_{lm},ΔS^{G}_{lm}, are residual Stokes coefficients, which have the background models (the GAD products) restored

and the degree 1 and J_2 coefficients corrected as described above. The post-processed basin averages (relative to the ocean bottom), $\widetilde{S}^g_{rsl}(t)$, are the result of a convolution of these Stokes coefficients with the filtered basin coefficients, $\tilde{\vartheta}_{lm}$. The symbol k_l denotes the load Love number and incorporates the change in gravity of the solid Earth induced by the surface load. The mean densities of water and the solid Earth are denoted by ρ_w and ρ_e respectively, and a is the mean radius of the Earth. The smoothing and truncation generally causes the true signal to be attenuated. This can be (partly) compensated by applying an a posteriori scaling factor $A_{\tilde{\vartheta}}$. The calculation of this factor requires knowledge of both the shape and size of the basin, of the applied smoothing and an hypothesis about the actual signal of interest. Practical values for $A_{\tilde{\vartheta}}$ are provided in section 2.2.

A comparison of GRACE- and altimetry-based mass-induced sea level requires to correct $\widetilde{S}^g_{rsl}$ for the load-induced ocean floor deformation, $\Delta\bar{u}$, as follows: $\widetilde{S}^g = \widetilde{S}^g_{rsl} + \Delta\bar{u}$. This correction is necessary since the altimeter orbits are given in a mean frame (i.e. realized by observations corrected for a certain time span) which does not dynamically change with the induced loading. The loading effect is deduced from the monthly GRACE geopotential coefficients and the load Love number h_l Farrell (1972) as follows:

$$\Delta\bar{u}(t) = A_{\tilde{\vartheta}} \frac{a}{\vartheta_{00}} \sum_{l=1}^{lmax} \sum_{m=0}^{l} \frac{h_l}{1+k_l} \{\tilde{\vartheta}^C_{lm} \Delta C^{G*}_{lm}(t) + \tilde{\vartheta}^{S*}_{lm} \Delta S^G_{lm}(t)\} \qquad (2)$$

In contrast to $\Delta C/S^G_{lm}$, $\Delta C/S^{G*}_{lm}$ also has the background models restored over land (using the GRACE-GAC product). The GAC product contains, as the GAD product, monthly averaged values of the oceanic model OMCT

and of the atmospheric model ECMWF. The main difference between the GAC and GAD products is that GAD does not include the atmosphere on land while GAC does, therefore in contrast to Eq. (1) we have restored here also the atmosphere over land. This ensures that the complete global load, including the continental atmosphere, is used in calculating the ocean floor deformation. Another difference between the GAC and the GAD products is in the way how the atmosphere is treated, as GAD contains surface pressure only while GAC contains vertically integrated atmospheric mass variation (Flechtner (2007a,b)). The latter difference is however not relevant, since the total load-induced ocean floor deformation, expressed in equivalent water heights, has an amplitude smaller than 8 millimeters in both basins and is therefore small compared to the GRACE-based mass variations (Tables 3, 4).

2.2. Spectral Filter

We may write the de-correlation filter in matrix notation as:

$$\widetilde{\mathbf{x}} = \mathbf{W}\mathbf{x} \tag{3}$$

with:

$$\mathbf{W} = (\mathbf{E^{-1}} + \alpha \mathbf{S^{-1}})^{-1}\mathbf{E^{-1}}$$

where vectors $\mathbf{x}$ and $\tilde{\mathbf{x}}$ contain the stacked Stokes coefficients of the unfiltered and filtered field respectively, $\mathbf{E}$ is an approximate block diagonal GRACE error covariance matrix (up to degree and order 100) and $\mathbf{S}$ a diagonal degree dependent signal covariance. The degree of smoothing is controlled by the parameter α. We use the anisotropic filter DDK3, with a degree of smoothing comparable to that of a Gaussian filter with a 300 km halfwidth

(Kusche et al. (2009)). The matrix $\mathbf{W}$ of the DDK3 filter is almost symmetric. Strictly speaking however, we must apply the transpose of $\mathbf{W}$ to the basin ϑ in order to obtain mathematically correct basin averages from equation 1. The resulting patterns of the smoothed basins kernel functions are shown in Figure 1.

The basin averaged time series have differences in the order of a few centimeters with respect to their Gaussian equivalents. The error of the monthly basin averages obtained using the DDK3 anisotropic filter and the Gaussian filters of half-width 300 km and 250 km is derived from the GRACE calibrated errors and shown in Figure 2. A large peak occurred in the second half of 2004 (most notably September 2004), when GRACE was in a near-repeat orbit causing large spatial gaps in the groundtrack pattern. For those months with decreased accuracy we use the constrained solutions, as provided by GFZ.

The filtering causes a reduction in the signal, which may be compensated by multiplying the filtered basin average values with a scale factor. The factor $A_{\tilde{\vartheta}}$ may be derived assuming a uniform signal distribution and computing the ratio of filtered and unfiltered field (Velicogna and Wahr (2006), Swenson and Wahr (2007)). Alternatively, $A_{\tilde{\vartheta}}$ is estimated as the average of the ratio of monthly unfiltered and filtered steric-corrected altimetric sea level averaged over the basin ($\frac{S^{a-s}_{mass}}{\widetilde{S}^{a-s}_{mass}}$) (Fenoglio-Marc et al. (2006)). The basin averages have been calculated in the spatial domain using the basin kernels from Figure 1. Both methods provide comparable factors (see Table 1), although they assume a different hypothesis for the signal. The damping is most pronounced

in the Black Sea due to its smaller area. The weakest damping corresponds to the simple truncation and depends on the chosen maximum degree. With the anisotropic filter DDK3 the factors are 1.39 and 1.4 in Mediterranean Sea and 1.62 and 1.7 in the Black Sea. Since the second method uses a more advanced hypothesis for the signal, we use the corresponding factors, 1.4 and 1.7 for the Mediterranean and Black Sea in the remainder of the paper.

2.3. Hydrological Leakage

The post-processing filter causes, in addition to the damping effect, also the leakage of mass signal from land in the seawater mass estimate. To correct for this effect, we estimate, according to Eq. (1) the smoothed basin averaged continental hydrological leakage $\widetilde{S}^h_{hyd}$ using various hydrological models. We consider three global hydrological models: the WaterGAP2 Global Hydrology Model (WG2), Döll et al. (2003), the Land Dynamics (LAD) Fraser model (Milly and Shmakin (2002)) and the Community Land Model of the Global Land Data Assimilation System (GLDAS-CLM, Rodell et al. (2004)). All monthly maps have been converted into sets of Stokes coefficients up to degree and order 100.

The hydrological leakage correction $\widetilde{S}^h_{hyd}$ is subtracted from the GIA-corrected (see Section 2.4) filtered GRACE-based mass variations $\widetilde{S}^g$ to obtain the hydrology-corrected smoothed GRACE solution $\widetilde{S}^{g-h}_{mass}$ ($\widetilde{S}^{g-h}_{mass} = \widetilde{S}^g - \widetilde{S}^h_{hyd}$). From a theoretical point of view, the correction is equivalent to subtracting the hydrological contribution directly from the GRACE coefficients before applying further post-processing.

2.4. Glacial Isostatic Adjustment

The Earth's surface is still viscously responding because of the surface unloading from melting of the late-Pleistocene ice sheets (e.g. Peltier (2004)). This phenomenon (referred to as Glacial Isostatic Adjustment (GIA)), depends upon the viscoelastic properties of the Earth. On the time scales of this study, GIA appears in GRACE data as a secular trend in the gravity field and will affect the estimates of ocean mass changes.

Using the open source program SELEN (Spada and Stocchi (2007)), the GIA correction has been calculated for a population of nine GIA models characterized by different viscosity profiles. The nine models have been obtained by perturbing the viscosity of the Earth model VM2 (Peltier (2004)) by $\pm$ 0.2×10^{21} Pa.s in the upper mantle and $\pm 2 \times 10^{21}$ Pa.s in the lower mantle. In all these experiments, the chronology of the ice sheets is unchanged. The GIA models provide the time-variations in coefficients from degree 2 to 128. For each model, we have computed the basin-averaged GIA rate expressed in equivalent water height. The procedure is consistent with the post-processing method applied to the GRACE data. Finally, the GIA correction is estimated by taking the mean of the values obtained from the population and we adopt the standard deviation of the results as an estimate for its error. In terms of equivalent water height, we obtain a GIA rate of -2.7$\pm$0.9 $^{\mathrm{mm}}/_{\mathrm{yr}}$ in the Mediterranean, and of -2.5$\pm$1.0 $^{\mathrm{mm}}/_{\mathrm{yr}}$ in the Black Sea. Even considering the errors, the values are generally larger than those reported by Paulson et al. (2007), whose model yield -1.64 $^{\mathrm{mm}}/_{\mathrm{yr}}$ for the Mediterranean and -1.1 $^{\mathrm{mm}}/_{\mathrm{yr}}$ for the Black Sea for a 300 km Gaussian smoothing. Investigating the cause of

the difference lies outside the scope of this paper. Nevertheless, the discrepancy indicates that GIA errors, when expressed in equivalent water height, may be larger than reported by Paulson et al. (2007) (20% of the signal) and of the same order of magnitude of the signal itself. The GIA correction is removed from the smoothed GRACE-based mass estimation $\tilde{S}^{g}_{mass}$. The GRACE-based mass-induced sea level basin average $\hat{S}^{g-h}_{mass}$ is then obtained after subtraction of the continental hydrological leakage correction $\widetilde{S}^{h}_{hyd}$ from $\tilde{S}^{g}_{mass}$ (Section 2.3) and after rescaling.

Since altimetry measures the geometrical surface height, we correct the altimetry-based sea level by removing the GIA component in terms of geoid changes (see Section 2.5). This correction is evaluated in SELEN accounting for both mass conservation and the variation of the geoid, from the same coefficients used above for GRACE. The resulting GIA geoid rate correction, expressed in basin averaged trends, is -0.34±0.1 $^{\mathrm{mm}}/_{\mathrm{yr}}$ in the Mediterranean Sea and -0.3±0.1 $^{\mathrm{mm}}/_{\mathrm{yr}}$ in the Black Sea.

2.5. Altimetric Sea Level Height

We estimate sea surface heights from Jason-1 and Envisat altimeter data. For this goal, we use the Radar Altimeter Database System (RADS) database, which provides an harmonized, validated and cross-calibrated set of altimeter data (Naeije et al. (2008)). We apply the conventional geophysical corrections (tides, wet and dry tropospheric correction, ionospheric correction, sea state bias) selecting the GOT4.7 ocean tide model, the radiometer wet tropospheric correction, the dry tropospheric correction from the ECMWF model, the dual-frequency ionosphere correction and the CLS sea state cor-

rection. On short time scales (< 30 days) the sea level response to surface pressure variations is far from an inverse barometer (Le Traon and Gauzelin (1997), Ducet et al. (1999)). We therefore account for the ocean response to atmospheric wind and pressure forcing (atmospheric loading on the sea surface) by applying the Dynamic Atmospheric Correction (DAC). This consists at low frequencies of the Inverse Barometer (IB) response and at high frequencies of the sea surface response simulated by the barotropic model MOG2D-G (Carrère and Lyard (2003)). Monthly equidistant grids with resolution of 0.25 x 0.25 degrees are then constructed from the merged data. Since the altimetry measurements include the change in geoid height due to GIA (see Section 2.4), we remove this contribution from the basin averages. For comparison, we use the basin-averaged sea level derived from the merged gridded delayed time products (Delayed Time Map of Sea Level Anomaly (DT-MSLA)) produced by SSALTO/DUACS and distributed by AVISO (http://www.aviso.oceanobs.com).

2.6. Steric component of sea level

We estimate the steric sea level variability in the Mediterranean Sea from the temperature and salinity fields of the regional Mediterranean Forecasting System ocean circulation model (MFSTEP) (Tonani et al. (2008)). This is a coupled monitoring and modelling system with enhancements in coastal regions that produces daily analyses and 10-day forecasts of currents and temperature and salinity fields at approximately 6.5 km spatial resolution. It is locally refined in four sub-regional areas with a resolution up to 3 km and in four shelf areas with a resolution of 1.5 km.

We have also computed steric heights using temperature and salinity from (1) the global ocean model ECCO/JPL kf080 (Fukumori et al. (2005)), and (2) from the global Ishii gridded climatologies, which are derived from hydrographic observations through objective analysis for the interval 1945-2006 (Ishii and Kimoto (2009)). Temperature and salinity error fields of the MEDAR climatology, available for the interval 1948-2002, have additionally been used to infer uncertainty estimates of the steric components (Rixen et al. (2005)).

In the Black Sea, we have estimated the steric sea level variability from the temperature and salinity fields of a regional ocean general circulation model (Grayek et al. (2010)) based on Nucleus for European Modelling of the Ocean (Foujols et al. (2000)), hereafter called NEMO. In horizontal direction the model uses an Arakawa C grid with a resolution of approximately 10 km (Stanev et al. (2003), Stanev et al. (2004)). The vertical grid uses hard-wired hyperbolic tangent stretching function with 31 levels. Horizontal boundaries are closed for Kerch Strait and open for the Bosphorus Strait. The model's initial conditions include vertical climatic profiles of temperature and salinity, the model forcing includes wind stress, air temperature and humidity constructed from atmospheric analysis data. Complete surface momentum and buoyancy forcing uses bulk aerodynamic formulae and simulated sea surface temperature (SST). River runoff R_B and Bosphorus FB exchange flow are also included. Altimeter data are assimilated in the model using the general concept of Cooper (1996). Basin mean sea level and hydrological forcing are combined to consistently close the water balance based

on Peneva et al. (2001). For comparison, we have also computed the seasonal steric sea level component from the World Ocean Atlas 2005 (WOA05) (http://www.nodc.noaa.gov) global climatology. The ECCO model and the Ishii database are not available in the Black Sea.

2.7. Precipitation, Evaporation and River Runoff

Oceanic evaporation and precipitation are challenging quantities to derive, as neither is directly observed. We have estimated basin means of monthly precipitation (P) from ECMWF precipitation data (temporal resolution 6 hours and spatial resolution 0.25°).

Basin means of monthly evaporation (E) have been estimated from ECMWF atmospheric data and simulated sea surface temperatures following the bulk formula from Stanev et al. (2003):

$$E = C_h|V| \times [e_{sat}(T_s) - re_{sat}(T_a)]\frac{0.622}{p_a} \tag{4}$$

where C_h is the drag coefficient (1.1×10^{-3}), V is the wind speed at 10 meters, r is the relative humidity at 2 meters and p_a atmospheric pressure at the sea surface. $e_{sat}(T_a)$ and $e_{sat}(T_s)$ are saturation vapour pressure at air temperature T_a, all derived from the ECMWF database, and sea surface temperature T_s simulated by the ocean models MFSTEP in the Mediterranean Sea and NEMO in the Black Sea.

For comparison, we have used alternative estimates of evaporation and precitation from ERA-Interim and DFS4 (DRAKKAR Forcing Set 4), an improved ERA40-based atmospheric forcing dataset (Brodeau et al. (2010)). We have also considered evaporation from the air-sea fluxes dataset OAFlux

(http://oaflux.whoi.edu), which objectively synthesizes surface meteorology obtained from satellite products and model reanalyses and precipitation from the Global Precipitation Climatology Project (GPCP, http://www.gewex.org).

The river runoff in the Mediterranean Sea, R_M, and in Black Sea, R_B, are obtained from the WaterGAP2 hydrology model. The river runoff R_B is alternatively estimated from a linear reconstruction based on yearly ECMWF precipitation over the ocean and from a seasonal climatology of river runoff according to Grayek et al. (2010). The linear reconstruction uses statistical rules of correlation between observed river runoff and precipitation data (Stanev and Peneva (2002)). The seasonal river runoff characteristics derived from the climatology are superimposed to the yearly estimation. Error estimates of the river runoff show that the reconstructed annual signal reflects most of the variability with an RMS error of 23% of the total variance.

2.8. Seasonal and Inter-Annual Variability

To examine the seasonal and long-term variability of the basin averages we have estimated annual, semi-annual and a linear trend component through a least-squares fit of the function :

$$m(t) = a_o + a_1 t + A_a cos(\omega_a t - \phi_a) + A_{sa} cos(\omega_{sa} t - \phi_{sa}) \qquad (5)$$

where a_o and a_1 are the parameters describing a bias and the linear component and A_i, ω_i, ϕ_i are amplitude, frequency and phase of the annual ($i = a$) and semiannual ($i = sa$) signals.

To examine the inter-annual variability of a time series we have removed

the seasonal component of the above least squares fit from the monthly values.

2.9. Sea level Budget and Strait flows

Since the total basin-wide sea level change S_{tot} is composed of a steric and of a mass part:

$$S_{tot} = S_{ster} + S_{mass} \tag{6}$$

we may use filtered altimetric sea level ($\widetilde{S}^a_{tot}$), steric sea level ($\widetilde{S}^s_{ster}$), GRACE ($\widetilde{S}^g$) and hydrological leakage from modelling, ($\widetilde{S}^h_{hyd}$), as well as their unfiltered (S^a_{tot}, S^s_{ster}) and filtered and rescaled equivalents ($\hat{S}^g$, $\hat{S}^h_{hyd}$) to close the mean sea level (MSL) budget in a semi-closed basin:

$$\widetilde{S}^a_{tot} = \widetilde{S}^s_{ster} + (\widetilde{S}^g - \widetilde{S}^h_{hyd}) \tag{7}$$

Since we have independent estimates for each component of Eq. 7, we may derive either an inferred or direct estimate for S_{tot}, S_{ster} and S_{mass}. The availability of all terms of Eq. 7 allows us to investigate whether the sea level budget in Eq. 6 is closed observationally, i.e. if the right and left side of the equation agree within the error estimates of each term (see also Willis et al. (2008)).

We compute the mass net flow from the Black Sea into the Mediterranean through the Bosphorus Strait, FB, using the water budget equation :

$$FB = -(E-P)_B + R_B - A_B(\dot{S}_{mass})_B \tag{8}$$

with R river runoff, $E-P$ evaporation minus precipitation, $\dot{S}_{mass}$ the rate of change of the mass induced sea level and A the surface area of the sea (see

also Grayek et al. (2010)). Similarly, the net flow in the Atlantic through the Gibraltar strait, FG, may be estimated using the water budget equation for the Mediterranean basin:

$$FG = (E - P)_M - R_M - FB + A_M(\dot{S}_{mass})_M \tag{9}$$

where the subscript $_M$ points to the Mediterranean equivalents of E, P, A and $\dot{S}_{mass}$.

For a basin with surface A, a uniform change of 1 $\frac{mm}{mon}$ is equivalent to a net flow of $0.38 \times 10^{-15} A$ Sv (1 Sv $= 10^6 m^3 s^{-1}$). This implies that 1 $\frac{mm}{mon}$ is equivalent to a net flow of 0.96×10^{-3} Sv in the Mediterranean Sea and of 0.16×10^{-3} Sv in the Black Sea. The water budget equations in Eq. 8, 9 can be written in terms of uniform basin changes (units are $\frac{mm}{mon}$) as :

$$(\dot{S}_{FB})_B = -(\dot{S}_{E-P})_B + (\dot{S}_R)_B - (\dot{S}_{mass})_B \tag{10}$$

$$(\dot{S}_{FG})_M = (\dot{S}_{E-P})_M - (\dot{S}_R)_M - (\dot{S}_{FB})_M + (\dot{S}_{mass})_M \tag{11}$$

where each component of Eq. 8, 9 has been divided by the surface area of the sea, $\dot{S}_{FG}, \dot{S}_{E-P}, \dot{S}_R, \dot{S}_{FB}, \dot{S}_{mass}$ indicate the uniform basin changes for each basin.

3. Results

3.1. Error estimation in terms of the Basin Averages

Estimated errors of the monthly values and annual amplitudes are tabulated in Table 7 for various measured and inferred quantities: total sea level (S_{tot}), steric sea level (S_{ster}), hydrological leakage (S_{hyd}), mass induced sea

level (S_{mass}) and its rate of change $\dot{S}_{mass}$, river runoff (R), $E-P$ and strait flows in terms of uniform basin changes.

The errors are based on either error propagation of the various components which flow into the estimated quantity, or they are based on the RMS difference between several models and/or data sets. The latter method, reflects the spread of the datasets, but unknown systematic errors may remain.

Monthly error estimates of the DDK3-filtered GRACE basin average ($\widetilde{S}^g$) have been discussed in Section 2.2. The errors are estimated to be around 11 mm in the Mediterranean Sea and 25 mm in the Black Sea.

The error in total altimetric sea level S^a_{tot}, is found to be 10 mm for the Mediterranean Sea and 30 mm for the Black Sea.

The error in the steric component, as measured by the oceanographic models (S^s_{ster}), is found to be 20 mm in the Mediterranean Sea. An RMS-based error of 13 mm has been derived from the temperature and salinity fields of both the MFSTEP and ECCO ocean models and of the Ishii hydrographic database, this latter reaches only a maximum depth of 600m. This shallow-water ocean error is lower than the yearly uncertainty of the steric component inferred from the temperature and salinity error fields derived from the MEDAR database climatology, which is below 15 mm in the 0-600 m layer and is mainly dominated by halosteric uncertainties (Fenoglio-Marc et al. (2012)). In order to account for the uncertainty of the deeper layers, we adopt a total error of 20 mm for the steric component arising from the

complete water column.

In the Black Sea, following Calafat et al. (2010), an error of 17 mm is used for the basin mean of the steric sea level simulated by NEMO. For comparison, the steric basin averages (S^s_{ster}) in the Black Sea from the NEMO model and the WOA05 climatology yield an error estimate of 14.6 mm. We have further validated the steric component derived from the NEMO model using ARGO temperature and salinity profiles available from the Global Data Assembly Centers (GDACs), however, the profiles are rather sparse and cover only the inner basin. Model simulations indicate that thermo-steric heights are dominating the basin-wide steric heights (Grayek et al. (2010)). In contrast, halo-steric heights are almost negligible in terms of basin averages (< 0.5 cm) and show a pronounced spatial variability. The error for the basin averaged steric sea level is based on a few sparse profiles and is most likely realistic for thermo-steric component only. We therefore neglect the halo-steric component in the Black Sea.

For the continental hydrological leakage correction ($\hat{S}^h_{hyd}$), we have estimated an error of 17 mm in the Mediterranean Sea and of 29 mm in the Black Sea. These estimates are based on the inter-comparison of the output from the WaterGAP2, GLDAS-CLM and LAD hydrology models.

A monthly error of $30\,{}^{\mathrm{mm}}/_{\mathrm{mon}}$, in the Mediterranean Sea, is considered for the surface water flux $\dot{S}_{E-P}$. This value has been derived from the mean of the root mean squares (RMS) differences between the $E-P$ used in this study

(e.g. computed from ECMWF and regional model data, see Section 2.7) and the $E - P$ given by two other databases, the ERA-Interim and the DFS4 databases. The RMS differences are 28 $^{\mathrm{mm}}/_{\mathrm{mon}}$ and 33 $^{\mathrm{mm}}/_{\mathrm{mon}}$ respectively.

Similarly, in the Black Sea the monthly error of 21 $^{\mathrm{mm}}/_{\mathrm{mon}}$ is derived as mean of the RMS differences between the $E - P$ computed from ECMWF and regional model data (Section 2.7) and the $E - P$ given by the two other databases (18 $^{\mathrm{mm}}/_{\mathrm{mon}}$ and 24 $^{\mathrm{mm}}/_{\mathrm{mon}}$ respectively).

The river runoff contribution to sea level ($\dot{S}_R$) in the Black Sea is found to have an error of 24 $^{\mathrm{mm}}/_{\mathrm{mon}}$, computed from the RMS difference between the reconstructed runoff and the runoff output of the WaterGAP2 model.

In the Mediterranean Sea, we have assumed a monthly error of 9 $^{\mathrm{mm}}/_{\mathrm{mon}}$, computed from the standard deviation of the runoff output of the WaterGAP2 model (an observed estimate was unfortunately not available).

3.2. Seawater mass estimates from corrected altimetry and GRACE

3.2.1. Mediterranean Sea

We first compare the mass-induced sea level derived from altimetry, S^{a-s}_{mass}, and the one derived from GRACE data, $\hat{S}^{g-s}_{mass}$, and select the most suitable steric and hydrology models.

In the Mediterranean Sea, the best agreement at seasonal and inter-annual scales between the basin averages is found with steric and hydrological leakage corrections derived from the regional ocean model MFSTEP in combination with the global hydrological model WaterGAP2 respectively (Table 2). Correlation and RMS differences are 0.86 and 37 mm for monthly time

series, are 0.85 and 15 mm for inter-annual components. The LAD/Fraser model yields a slightly higher agreement (correlation and RMS differences are 0.91 and 25 mm for monthly time series, and 0.89 and 12 mm for the inter-annual components) but is available only until the end 2006 and, for this reason, will not be used here.

The mass induced sea level from GRACE has an annual amplitude of 27±5 mm peaking around 18^{th} December (Table 3). Compared to the altimetry-derived S^{a-s}_{mass} (annual amplitude of 24±3 mm peaking around 24^{th} November) it is consistent within 3 mm and 23 days in terms of the annual amplitude and phase (Table 2). When we apply the continental hydrological leakage correction from GLDAS-CLM to GRACE, the agreement between the series is reduced (for all available choices of the steric correction).

Figure 3 (top) graphically shows annual amplitudes and phases of the observed and inferred parameters (mass, steric- and continental hydrological leakage correction), for a variety of hydrological models (WaterGAP2, LAD, GLDAS) and steric corrections (MFSTEP, ECCO, Ishii). From the possible combinations, the mass estimates corresponding to MFSTEP and WaterGAP2 corrections have the best agreement over the complete interval. Better agreement may have been obtained by either increasing the amplitude of the steric correction to 66±4 mm, or by increasing the amplitude of the leakage of continental hydrology to 34±4 mm (empty markers in Figure 3) while keeping the other correction fixed.

We note that all selections of the steric and continental hydrological leakage corrections suggest a significant increase of oceanic mass. The altimetry-based and the GRACE-based mass estimates almost agree within the error bounds of the altimetry-derived mass estimate (Figure 4.a). The discrepancy between the two estimates is most visible in the trend. The trend of the selected hydrology-corrected GRACE solution is $5.3\pm1.9\,{}^{\mathrm{mm}}/_{\mathrm{yr}}$, while the trend of the altimetry-derived mass deviates by $3\,{}^{\mathrm{mm}}/_{\mathrm{yr}}$, which is larger than the calculated error bar (Table 3).

Using the MFSTEP steric correction and the WaterGAP2 hydrological correction, we compare, for each component entering the MSL budget (S_{ster}, S_{mass}, S_{hyd}, S_{tot}, Eq. 7), the direct estimate given by the observations and the inferred one from the other components (Figure 4.b-e, and Table 3). The observational estimate of each term are shown as black lines and their error bounds are in light gray. The dark gray lines represent inferred estimates of each term, computed by adding or subtracting the other three, as in Eq. 7.

The total sea level as observed from altimetry is shown in Figure 4.b. The dominant seasonal signal displays an amplitude of $70\pm2\,\mathrm{mm}$ and a phase of 278 ± 4 days (peak around 4^{th} October). The trend is not significant ($0.8\pm1.3\,{}^{\mathrm{mm}}/_{\mathrm{yr}}$). Its inferred estimate is obtained by the addition of the steric component to the GRACE-based mass induced sea level. The seasonal and inter-annual fluctuations of the inferred estimate are similar to those of the observational estimates. The amplitude of the seasonal cycle is slightly lower for the inferred estimate and does not agree within the expected observational error bounds. The primary difference appears to be

498 in the trend, which is -4.0±2.9 $^{mm}/_{yr}$ for the inferred estimate and therefore
499 4.8 $^{mm}/_{yr}$ smaller than the trend of the altimeter, it is outside of the error
500 bounds of the altimeter-based observations.
501
502 The steric component is given in Figure 4.c. Its inferred estimate is
503 obtained by the subtraction of the GRACE-derived mass from the altime-
504 try derived sea level (S^a_{tot}). Both the direct estimates, derived from MF-
505 STEP, ECCO and Ishii, and the inferred estimate have an annual amplitude
506 peaking in September (see Table 3). The agreement in phase is remarkably
507 good (peak on 17 or 18 September for the direct observations and between
508 5 and 13 September for the inferred estimates). The amplitude varies be-
509 tween 58±4 mm (MFSTEP) and 48±4 mm (ECCO), while the inferred es-
510 timate has a larger amplitude that depends on the hydrological model used
511 (66±4 with WaterGAP2 and 80±4 with GLDAS). All estimates of steric sea
512 level have significant negative trends, with the highest value for MFSTEP
513 (-10.1±0.6 $^{mm}/_{yr}$ (MFSTEP), -3.1±0.4 $^{mm}/_{yr}$ (ECCO), -5.8±0.4 $^{mm}/_{yr}$ (Ishii)).
514 The trends of the inferred estimates are -5.3±1.1 $^{mm}/_{yr}$ with WaterGAP2 and
515 -3.1±1.2 $^{mm}/_{yr}$ with GLDAS.
516
517 The inferred estimate of continental hydrological leakage, $S^{g-(a-s)}_{hyd}$, is ob-
518 tained by subtraction of the mass-induced sea level derived from altimetry
519 from the rescaled GRACE basin average (Figure 4.d). All direct and in-
520 ferred estimates have a dominant annual signal with amplitude peaking in
521 February-March and agreement in phase within 12 days. The annual ampli-
522 tude ranges from 10±4 mm (GLDAS) to 32±4 mm (LAD) and is 27±3 mm

for WaterGAP2. The inferred continental hydrological leakage (using the steric MFSTEP correction) has an annual amplitude larger than all direct estimates (34±4 mm). Its phase agrees well with WaterGAP2 and is within the errors for all estimates. All trends are negative, with the highest value corresponding to the inferred estimate (-8.7±2.1 $^{\mathrm{mm}}/_{\mathrm{yr}}$) and lower values for direct estimates (-1.0±0.6 $^{\mathrm{mm}}/_{\mathrm{yr}}$ for WaterGAP2, -0.7±0.6 $^{\mathrm{mm}}/_{\mathrm{yr}}$ for GLDAS-CLM -1.0±0.6 $^{\mathrm{mm}}/_{\mathrm{yr}}$ for LAD).

The total mass observed by GRACE, $\hat{S}^g$, is shown in Figure 4.e. Both the direct estimates derived from GRACE and the inferred estimate, obtained by subtraction of S^{a-s}_{mass} from the smoothed and rescaled continental hydrological leakage correction $\hat{S}^h_{hyd}$, have a strong annual signal. The amplitude of the GRACE direct observation is 46±4 mm and peaks in January. Applying the continental hydrological leakage correction to GRACE reduces the strength of its seasonal signal: the annual amplitude is smaller and its maximum, initially in January, is shifted forward by about one month. Similarly, the removal of the steric signal from the altimetric sea level, causes a reduction of the amplitude of the altimeter sea level and its maximum, initially in October, is delayed by about one month (Figure 4.a).

Figure 6 depicts the inter-annual mass change. All choices of the hydrology model give similar results for the inter-annual mass induced sea level derived from altimetry, S^{a-s}_{mass} and from GRACE, $\hat{S}^{g-h}_{mass}$, with correlation higher than 0.66 and RMS of the differences smaller than 21 mm (see Table 2).

From the above discussion we find that the interval 2002-2008 has been characterized by a positive trend in the mass-induced sea level S_{mass} ($5.3\pm1.9\,^{\mathrm{mm}}/_{\mathrm{yr}}$ from $\hat{S}^{g-h}_{mass}$) and by a negative trend in the steric sea level S_{ster} (e.g. -$5.3\pm1.1\,^{\mathrm{mm}}/_{\mathrm{yr}}$ for S^{a-g+h}_{ster}). In contrast, the trend in the observed total sea level S_{tot} was not significant ($0.8\pm1.3\,^{\mathrm{mm}}/_{\mathrm{yr}}$).

Figure 7 shows for an extended interval, the 1993-2008 period, the total basin-wide sea level together with its two components (steric and mass component). Additionally, the steric component has been split up in a thermosteric and halo-steric part. During the complete interval 1993-2008, the total sea level has a positive trend of $2.0\pm1.2\,^{\mathrm{mm}}/_{\mathrm{yr}}$. The trend was higher during the sub-interval 1993-2002 ($3.9\pm2.5\,^{\mathrm{mm}}/_{\mathrm{yr}}$) compared to the following years, and not significant over the period 2002-2006 (-$0.6\pm0.8\,^{\mathrm{mm}}/_{\mathrm{yr}}$). Both the Ishii and the Medar databases indicate an increase of the steric component in 1993-2000, a feature which is missing in the ECCO model. Beginning in the year 2000, we see a better agreement in the steric components derived from various sources, namely a decrease in the sub-interval 2000-2005 and an increase afterwards are common features for both the Ishii and the Medar hydrographic databases as well as for the ECCO and MFSTEP ocean models (Figure 7.c).

The mass-induced sea level S^{a-s}_{mass} derived from steric-corrected altimetry using the ECCO model increases in 1994-1996 and shows a similar increase in 2002-2006 (Figure 7.b). The same behaviour is obtained from the Ishii data neglecting their halo-steric component. We conclude that, as the accu-

racy of the halo-steric component is low (Ishii personal communication), its inclusion has to be considered with care (Ishii and Kimoto (2009)).

All sources indicate a relative minimum in water-mass anomaly in 2000-2002. In summary, the rise in sea level observed by satellite altimetry in the 1990's appears to arise from both thermal expansion and mass addition. In the following decade (2000-2010) the increase in mass has been compensated by the decrease in steric sea level and for this reason the rise of sea level has been less pronounced.

3.2.2. Black Sea

The regional model NEMO is the only model available in the Black Sea to compute the steric correction. To select the most suitable hydrology model, we have first compared the altimetry-derived S^{a-s}_{mass} with the $\hat{S}^{g-h}_{mass}$ obtained from GRACE using several hydrological corrections. As shown in Figure 3, the best agreement at seasonal and inter-annual scales between the two estimates of oceanic mass is obtained by using the correction from WaterGAP2. Correlation and RMS differences are 0.71 and 120 mm respectively, and 0.68 and 55 mm for the inter-annual monthly values (Table 2). The annual component remains the dominant signal in the steric and continental hydrological leakage corrections, but in S_{tot}, and S_{mass} also the semi-annual signals become important (Table 4).

The GRACE-derived mass-induced sea level, $\hat{S}^{g-h}_{mass}$ shows an annual signal of 35±5 mm amplitude peaking around 11^{th} April and a semi-annual signal 45±4 mm amplitude peaking in May (Table 4). Their consistency with the

altimetry-derived mass-induced sea level S^{a-s}_{mass} (annual signal of 32±5 mm amplitude peaking around 20^{th} April) is within 3 mm and 9 days for annual amplitude and phase but lower for semi-annual amplitudes (within 12 mm and 16 days). Compared to the hydrological correction from WaterGAP2, the correlation and RMS differences of the monthly values are worsened when we use GLDAS-CLM (0.69 and 66 mm for monthly time series, and 0.64 and 60 mm for inter-annual time series). Differences between annual and semi-annual amplitudes and phases are also larger (20 mm, 22 days and 3 mm, 12 days respectively, Table 2).

Similar to Fig.4, Fig. 5.a-e shows, for the Black Sea, the direct and the inferred estimates for each component of the basin MSL budget equation (Eq. 7). The agreement of the mass induced sea level is weaker compared to the time series in the Mediterranean Sea.

The total sea level, S^{a}_{tot}, as observed from satellite altimetry, is shown in Figure 5.b. Annual and semi-annual signals are smaller than in the Mediterranean Sea (with amplitudes 23±4 mm and 28±4 mm), the annual signal peaks in June.

Both the steric component derived from NEMO, S^{s}_{ster}, and the inferred estimate, S^{a-g+h}_{ster}, have an annual amplitude peaking end of August (Figure 5.c, Table 4). The agreement in phase is remarkably good, although the NEMO estimate is much smoother compared to the inferred estimate. The annual amplitude is 35±4 mm for NEMO and 29±4 mm for the mean

seasonal climatology. The amplitude of the inferred estimates is 40±5 mm and therefore larger than the NEMO model value. The estimated trends (-0.3±0.6 $^{\mathrm{mm}}/_{\mathrm{yr}}$, 0.2±1.1 $^{\mathrm{mm}}/_{\mathrm{yr}}$) are not significant (Table 4).

The direct estimate of the continental hydrological leakage derived from WaterGAP2, LAD, GLDAS and the inferred estimate, $S_{hyd}^{g-(a-s)}$, all show an annual amplitude peaking in February (Figure 5.c). The dominant signal is annual, with an amplitude ranging from 40±4 mm for GLDAS to 106±10 mm for LAD, while WaterGap2 yields 68±7 mm. The agreement in phase is within 10 days. Significantly different trends have been found for the different models (-3.2±0.6 $^{\mathrm{mm}}/_{\mathrm{yr}}$ for GLDAS-CLM, -0.3±0.6 $^{\mathrm{mm}}/_{\mathrm{yr}}$ for WaterGAP, 1.3±0.6 $^{\mathrm{mm}}/_{\mathrm{yr}}$ for LAD)(Table 4) .

The total mass-induced sea level, $\hat{S}^g$, observed by GRACE is shown in Figure 5.e. Both the direct estimates derived from GRACE and the inferred estimate, obtained by subtraction of the altimetry-derived mass-induced sea level from the rescaled continental hydrological leakage have a strong annual signal. The amplitude of the GRACE direct observation is 97±10 mm and peaks in March. Similar to the Mediterranean, the removal of the leakage signal reduces the annual amplitude of the GRACE time series and delays its maximum, from March to the end of April (peak around 29^{th} April, Fig. 5.a). Considering the long-term behavior, the interval 2002-2008 is characterized by an inter-annual signal corresponding to a mass increase in 2003-2005 and mass decrease in 2006-2008. Figure 6 shows that results are similar for all choices of the hydrology model. The correlation with the altimetry-derived

estimate is larger than 0.5 and the RMS of the differences is smaller than 60 mm (Table 2).

3.3. Mass fluxes and Strait flows

Using a simple numerical two point differentation, we can estimate the water mass change per month $\dot{S}_{mass}$, from either steric corrected altimetry or hydrology-corrected GRACE data, where the latter method is independent from oceanographic modelling. In the Mediterranean Sea, the GRACE-derived $\dot{\hat{S}}^{g-h}_{mass}$ shows an annual signal with amplitude $16\pm5\,^{\mathrm{mm}}/_{\mathrm{mon}}$ (16 ± 5 10^{-3} Sv) peaking around the 27^{th} September (Figure 8.d and Table 5). In the Black Sea, $\dot{\hat{S}}^{g-h}_{mass}$ has maximum amplitude in March with a strong semi-annual component, in addition to the annual component (Figure 9.d and Table 6).

Figures 8.a, 9.a show that evaporation exceeds precipitation in both basins. The annual amplitudes of $E-P$, in terms of uniform layer of water in the basins, are $19\pm5\,^{\mathrm{mm}}/_{\mathrm{mon}}$ ($19\pm5\times10^{-3}$ Sv) for the Mediterranean and $40\pm5\,^{\mathrm{mm}}/_{\mathrm{mon}}$ ($6\pm1\times10^{-3}$ Sv) for the Black Sea and peak at the same time (around the 20^{th} September)(Tables 5 and 6). In the Mediterranean Sea, our estimate of $E-P$ has a bias compared to the DFS4 and ERA-Interim results, whereas it has no bias compared to the OAFLUX-GPCP derived quantities. In the Black Sea the agreement is very good for all estimates (Figures 8.b, 9.b). River runoff is the smallest component in the Mediterranean Sea, while it is comparable to $E-P$ in the Black Sea (Figures 8.c, 9.c). Consequently, the freshwater budget $E-P-R$ displays mostly posi-

tive values in the Mediterranean Sea (deficit) and alternating values in the Black Sea.

Figure 10 (bottom) shows the net mass outflow FB through the Bosphorus Strait computed from Eq.8. The seasonal cycle of the GRACE-derived estimate $\dot{S}_{FB}^{g-h}$ (contributes to a layer change of $83\pm18\,{}^{\mathrm{mm}}/_{\mathrm{mon}}$ ($13\pm3\times10^{-3}$ Sv) peaking around the 28^{th} March (Figure 9). FB has a larger annual amplitude than the river runoff R_B and vertical surface water flux $(E-P)_B$ (Table 6, see also Stanev et al. (2000)).

In the Mediterranean Sea, the vertical surface water flux $(E-P)_M$ contributes at seasonal scales to a layer change $\dot{S}_{E-P}$ of $19\pm2\,{}^{\mathrm{mm}}/_{\mathrm{mon}}$ peaking middle of September, which is larger than the net mass flow through the Bosphorus Strait FB and the river runoff R_M (Table 5).

Figure 10 (top) shows the Gibraltar flux computed from Eq. 9. Its annual cycle peaks in the middle of September, in phase with the annual component of $(E-P)_M$. The contribution of $(E-P)_M$ to FG is dominant, while contributions from R_{Med} and FB are smaller. All estimations of FG using all combinations of mass change estimation from hydrology-corrected GRACE and from steric-corrected altimetry yield a mass flow FG with an annual amplitude of about $54\pm10\,{}^{\mathrm{mm}}/_{\mathrm{mon}}$ ($52\pm10\times10^{-3}$ Sv) peaking in September-October (Table 5). Trends are positive for both the $E-P$ ($2.4\pm0.3\times10^{-3}\,{}^{\mathrm{Sv}}/_{\mathrm{yr}}$) and the FG GRACE-derived estimate ($3.4\pm0.8\times10^{-3}\,{}^{\mathrm{Sv}}/_{\mathrm{yr}}$), in agreement with Fenoglio-Marc et al. (2012).

In Section 3.1, we have discussed the monthly errors adopted in this study. The monthly error of the combined mass-induced sea level S_{mass} and of the strait flow FB and FG, estimated above, have been derived from uncorrelated error propagation of each components. We find that in the Mediterranean Sea monthly basin averages of GRACE- and altimetry-derived S_{mass} have comparable accuracy (23 and 22 mm). In the Black Sea, $\hat{S}^{g-h}_{mass}$ has a lower accuracy (51 mm) compared to the altimetry-derived S^{a-s}_{mass} (35 mm) (Table 7). Consequently, our GRACE-derived estimate of the Bosphorus strait flow FB yields a lower accuracy ($78\,^{\mathrm{mm}}/_{\mathrm{month}}$, with a contribution of $72\,^{\mathrm{mm}}/_{\mathrm{month}}$ from $\dot{\hat{S}}^{g-h}_{mass}$) compared to the altimetry-derived FB ($58\,^{\mathrm{mm}}/_{\mathrm{month}}$).

The accuracy of the Gibraltar strait flow FG ($47\,^{\mathrm{mm}}/_{\mathrm{month}}$) is almost independent of the computed Bosphorus flow, as its effect is small in the overall estimate. In contrast, the uncertainties of the Mediterranean $E - P$ ($30\,^{\mathrm{mm}}/_{\mathrm{month}}$) and $\dot{\hat{S}}^{g-h}_{mass}$) ($33\,^{\mathrm{mm}}/_{\mathrm{month}}$) propagate most strongly into the uncertainty of the strait flow at Gibraltar.

4. Conclusions and Discussion

We have investigated the mass induced sea level S_{mass} in the Mediterranean and Black Sea basins over an interval of six years, from August 2002 to July 2008, at both seasonal and inter-annual time scales. In addition to Fenoglio-Marc et al. (2006), Fenoglio-Marc et al. (2007), we have used estimates derived from GRACE and altimetry to study the closure of the water budget in both the Mediterranean and Black Sea. Furthermore, by applying

conservation of mass, the estimates have been used to derive strait flows at Gibraltar and through the Bosphorus.

The comparison required the use of a variety of auxiliary data. Hydrological models were considered to estimate the continental leakage correction to the GRACE gravity observations and oceanographic models and data to derive the steric correction to the altimetric sea level observations. The closure of the water budget additionally required the use of estimates of evaporation, precipitation and river runoff.

First we have analyzed the consistency between the basin mean of S_{mass} derived from GRACE and altimetry data and have selected the most suitable steric and continental hydrological leakage corrections. We have found that the corrections yielding the best agreement at seasonal scales (i.e. smallest difference in annual amplitude and phase, smallest standard deviation of the differences and highest correlation) are those derived from the WaterGAP2 hydrological model and the MFSTEP regional ocean model in the Mediterranean Sea, and those derived from the WaterGAP2 hydrological model and the NEMO regional ocean model in the Black Sea.

In the Mediterranean Sea, the agreement in annual phase is not perfect, and our work suggests that the annual signal in either the steric correction and/or the hydrological correction is underestimated. A single hydrology model (CPC, Fan and van der Dool (2004)) and one steric database (Ishii, Ishii and Kimoto (2009)) were considered by Calafat et al. (2010), who found

both estimations of annual ocean mass peaking in October. Similarly, Garcia et al. (2010) use only one hydrology model (GLDAS) but a variety of ocean models and ocean data. These authors give an estimation of annual ocean mass peaking in January and report on the best agreement with GLDAS realized by an ideal steric component with large amplitude (77 mm). They further identify the Mercator model as the best existing model (steric correction with amplitude 68 mm) .

We have shown here that, while for each hydrologic model chosen a "best" steric correction exist, the errors are most likely to arise from the combination of both corrections. Using the "best" existing corrections we have identified for the Mediterranean Sea, we find that the annual amplitude and phase of the GRACE- and altimetry-based mass-induced sea level basin average, $\hat{S}^{g-h}_{mass}$ and S^{a-s}_{mass}, agree within 3 mm and 23 days and that the monthly time series peak in December. Correlation and RMS difference are 0.86 and 37 mm for the monthly time series and 0.85 and 15 mm for the inter-annual time series. The best agreement with WaterGAP2 is realized by an ideal steric component with larger amplitude (66 mm) than the MFSTEP annual correction (amplitude 58 mm). There is an excellent agreement both at seasonal and inter-annual time scales. The accuracy of $\hat{S}^{g-h}_{mass}$ and S^{a-s}_{mass} is comparable, 23 and 22 mm respectively and the time-series agree within the error bounds.

In the Black Sea, using the 'best' correction identified, the estimated $\hat{S}^{g-h}_{mass}$,S^{a-s}_{mass} are less consistent than in Mediterranean Sea and do not always agree within the error bounds of the altimetry-derived mass estimate. We

find that the consistency at seasonal scales is within 4 mm and 6 days for seasonal amplitude and phase, the time series peak in April. Correlation and RMS differences are 0.68 and 55 mm for monthly time series and 0.71 and 65 mm for the inter-annual time series. The accuracy is lower for the monthly basin averaged $\hat{S}^{g-h}_{mass}$ derived from GRACE (52 mm) than for the altimetry-derived S^{a-s}_{mass} (39 mm). Considering the small size of the Black Sea in relation to the GRACE spatial resolution, and despite the large magnitude of the hydrological correction, this is a promising agreement.

Also new in this paper is the analysis of the trends in S_{mass}, which depend on the choice of the GIA correction and of the steric and hydrological corrections. We have estimated an error of $0.9\,{}^{\mathrm{mm}}/_{\mathrm{yr}}$ for the GIA correction in terms of equivalent water height, based on different choices of parameters for the GIA model as well as on a comparison with published results.

Nevertheless, we have identified the steric component as the main source of the uncertainty in the trend of the altimetry-derived S^{a-s}_{mass} in the Mediterranean Sea. Differences in the trends of the steric correction derived from the ocean models are up to $5\,{}^{\mathrm{mm}}/_{\mathrm{yr}}$ ($2.9 \pm 1.6\,{}^{\mathrm{mm}}/_{\mathrm{yr}}$ using ECCO and $8.3 \pm 1.6\,{}^{\mathrm{mm}}/_{\mathrm{yr}}$ with MFSTEP). Additionally, the choice of the continental hydrological leakage correction affects the trend of the GRACE-derived $\hat{S}^{g-h}_{mass}$, with differences up to $3\,{}^{\mathrm{mm}}/_{\mathrm{yr}}$ when using different hydrological models. Trends are found to be $2.8 \pm 1.9\,{}^{\mathrm{mm}}/_{\mathrm{yr}}$ when using GLDAS versus $5.3 \pm 1.9\,{}^{\mathrm{mm}}/_{\mathrm{yr}}$ when using WaterGap2. The trend of the GRACE-derived steric sea, S^{a-g+h}_{ster} is -5.3±1.1 ${}^{\mathrm{mm}}/_{\mathrm{yr}}$, which lies between the values of altimetry-derived trends using the ECCO

797 and MFSTEP steric corrections.

798

799 The analysis over longer time periods suggests that significant inter-
800 annual variations occur in both the mass and steric components of sea level.
801 We have shown that in the Mediterranean Sea, a period of rise in total sea
802 level, caused by a rise of both the steric and mass induced sea level occurred
803 in the 90's. In the subsequent decade the situation changed, as the increase
804 in mass was compensated by the steric sea level, resulting in a more or less
805 constant total sea level rise.

806 In the Black Sea, the inter-annual variability of S_{mass} is stronger than
807 the Mediterranean Sea, with an increase in 2003-2005 followed by a decrease
808 in 2006-2008. The annual signal has amplitude of 32±5 mm peaking in April.

809

810 The Bosphorus net flow derived from GRACE yields an annual ampli-
811 tude of $13\pm4\times10^{-3}$ Sv in terms of volume transport peaking end of March
812 ($81\pm18\,^{\mathrm{mm}}/_{\mathrm{mon}}$ in terms of uniform layer change in the Black Sea and $13\pm4\,^{\mathrm{mm}}/_{\mathrm{mon}}$
813 in terms of uniform layer change in the Mediterranean Sea). The GRACE-
814 based and the altimetry-based Bosphorus net flow agree within the error
815 bounds of the altimetry-based estimate. The accuracy of $\dot{S}_{FB}^{g-h}$ is lower than
816 the accuracy of $\dot{S}_{FB}^{a-s}$, due to the lower accuracy of the GRACE-based mass
817 estimate in the Black Sea.

818 The Gibraltar Strait flow derived from GRACE has an annual amplitude
819 of $52\pm11\times10^{-3}$ Sv in terms of volume transport peaking in September-
820 October ($52\pm11\,^{\mathrm{mm}}/_{\mathrm{mon}}$ in terms of uniform layer in the Mediterranean Sea).
821 Values are slightly smaller than those derived from current meter measure-

822 ments Garcia Lafuente et al. (2002) (annual amplitude of the water flux
823 78 $^{mm}/_{mon}$ peaking in September) and agree with results reported by other
824 authors Garcia et al. (2006, 2010). Also in this case, the GRACE-based and
825 the altimetry-based net flow agree within the error bounds of the altimetry-
826 based estimate. Here, however, the accuracy of the Gibraltar Strait flow is
827 virtually independent of the mass change used in computing the Bosphorus
828 net flux, as the effect of this strait flow is small in the estimate of the Gibral-
829 tar net flux. Moreover, both the GRACE-based Gibraltar Strait flow and
830 the altimetry-based Gibraltar net flow have comparable accuracy, due to the
831 comparable accuracy of the GRACE- and altimetry-derived mass estimate
832 in the Mediterranean Sea.
833
834 We conclude that, although resolution and accuracy of the mass-induced
835 sea level estimate have been improved by using the latest GRACE models
836 and the improved filtering methods, results are still dependent on the accu-
837 racy of the auxiliary data and models used to compute the corrections. The
838 cross validation performed in this study is a viable tool to asses those errors
839 and improve them in future studies.
840
841 An improved regional hydrology model, incorporating anthropogenic wa-
842 ter use models, is currently under development (Aus der Beek et al. (2012),
843 this issue). This model will provide valuable insights in the hydrology of the
844 complete watershed region draining in the Black Sea and Mediterranean Sea.
845 At the same time, it will be able to provide river runoff forcing for the ocean
846 models, and supply hydrological corrections for GRACE.

Acknowledgments

The authors acknowledge G. Spada for the GIA corrections, A. Güntner for the WaterGAP2 data, B. Barnier and R. Dussin for support on DFS4 and ERA-Interim airflux data, M. Rixen and A. Shaw for helpfull discussions on the MEDAR/Medatlas data. Comments by W. Bosch and by two anonymous reviewers helped to improve the manuscript. This study has been performed within the STREMP project funded by the Deutsche Forschungsgemeinschaft SPP1257 (FE-534/3-2).

References

Beckley, B.D., Lemoine, F.G., Luthcke, S.B., Ray, R.D., Zelensky, N.P., 2007. A reassessement of global and regional mean sea level trends form TOPEX and Jason-1 altimetry based on revised reference frame and orbits. Geoph. Res. Lett. 34.

Aus der Beek, T., Menzel, L., Grayek, S., Rietbroek, R., Fenoglio-Marc, L., Becker, M., Kusche, J., Stanev, E., 2012. Modelling the water resources of the Black and Mediterranean Sea river basins and their impact on regional mass changes. J. of Geodynamics 10.1016/j.jog.2011.11.011.

Brodeau, L., Barnier, B., Treguier, A.M., Penduff, T., Gulev, S., 2010. An ERA40-based atmospheric forcing for global ocean circulation models. Ocean Modelling 31, 88104.

868 Calafat, F., Marcos, M., Gomis, D., 2010. Mass contribution to Mediter-
869 ranean Sea level variability for the period 1948-2000. Global and Planetary
870 Change .

871 Carrère, L., Lyard, F., 2003. Modeling the barotropic response of the global
872 ocean to atmospheric wind and pressure forcing - comparisons with obser-
873 vations. Geoph. Res. Lett. 30, 8–1.

874 Chambers, D.P., 2006. Observing seasonal steric sea level variations with
875 GRACE and satellite altimetry. J. Geophys. Res. 111, 3010.

876 Cheng, M., Tapley, B., 2004. Variations in the Earth's oblateness during the
877 past 28 years. J.Geophys. Research 109, B09402.

878 Cooper, M., K.H., 1996. Altimetric assimilation with water property conser-
879 vation. J. Geophys. Res. 101 (C1), 1059–1077.

880 Döll, P., Kaspar, F., Lehner, B., 2003. A global hydrological model for
881 deriving water availability indicators: model tuning and validation. J. of
882 Hydrology 207, 105–134.

883 Ducet, N., Le Traon, P., Gauzelin, P., 1999. Response of the Black Sea mean
884 level to atmopheric pressure and wind forcing. J. of Marine Systems 22,
885 311–327.

886 Fan, Y., van der Dool, H., 2004. Climate prediction center global monthly soil
887 moisture data set at 0.5 degree resolution for 1948 to present. J. Geophys.
888 Res 109, doi:10.1029/2003JD004345.

889 Farrell, W.E., 1972. Deformation of the Earth by Surface Loads. Reviews of
890 Geophysics and Space Physics 10, 761.

891 Fenoglio-Marc, L., Kusche, J., Becker, M., 2006. Mass variation in
892 the Mediterranean Sea from GRACE and its validation by altime-
893 try, steric and hydrologic fields. Geophys. Res. Lett. 33, L19606,
894 doi:10.1029/2006GL026851.

895 Fenoglio-Marc, L., Kusche, J., Becker, M., I., F., 2007. Comment on "On
896 the steric and mass-induced contributions to the annual sea level variations
897 in the Mediterranean Sea" by David García et al. J. Geophys. Res. 112,
898 C12018, 10.1029/2007JC004196.

899 Fenoglio-Marc, L., Mariotti, A., Sannino, G., Meyssignac, B., Carillo, A.,
900 Struglia, M.V., 2012. Decadal variability of the net water flux at the
901 Mediterranean Sea Gibraltar Strait. Global and Planetary Change sub-
902 mitted.

903 Flechtner, F., 2007a. AOD1B Product Description Document for Product
904 Release 01 to 04. GRACE 327-750, GR-GFZ-AOD-0001.

905 Flechtner, F., 2007b. GFZ level-2 processing standards document for level-2
906 product release 0004. GRACE 327-743, Rev. 1.0.

907 Foujols, M., Levy, M., Aumont, O., Madec, G., 2000. OPA 8.1 Tracer Model
908 reference manual. Note du Pole de modlisation. Technical Report. Institut
909 Pierre-Simon Laplace (IPSL), France, 45 pp.

910 Fukumori, I., Menemenlis, D., Lee, T., 2005. A Near-Uniform Basin-Wide
911 Sea Level Fluctuation of the Mediterranean Sea. J. Phys. Oceanogr. .

912 Garcia, D., Chao, B., Boy, J.P., 2010. Steric and mass-induced sea level vari-
913 ations in the Mediterranean Sea revisited. J. Geophys. Res. 115, C12016.

914 Garcia, D., Chao, B., Del Rio, J., Vigo, I., Garcia-Lafuente, J., 2006. On the
915 steric and mass induced contributions to the annual sea level variations in
916 the Mediterranean Sea. Global and Planetary Change .

917 Garcia Lafuente, J.G., Delgado, J., Vergas, M., Plaza, F., Sarhan, T., 2002.
918 Low frequency variability of the exchanged flows throught the Strait of
919 Gibraltar during CANIGO. Deep Sea Res. 49, 4051–4067.

920 Grayek, S., Stanev, E.V., Kandilarov, R., 2010. On the Response of Black
921 Sea Level to External Forcing: Altimeter Data and Numerical Modelling.
922 Ocean Dynamics 60, 123–140.

923 Han, S.C.S., Jekeli, C., Kuo, C., Wilson, C., Seo, K., 2005. Non-isotropic
924 filtering of GRACE temporal gravity for geophysical signal enhancement.
925 Geophys. J. Int. 163, 18–25.

926 Ishii, M., Kimoto, M., 2009. Reevaluation of Historical Ocean Heat Content
927 Variations with Time-Varying XBT and MBT Depth Bias Corrections. J.
928 of Oceanography 65, 587–299.

929 Klees, R., Zapreeva, E., Winsemius, H., Savenije, H., 2007. The bias in
930 GRACE estimates of continental storage variations. Hydrology and Earth
931 System Sciences 11, 1227–1241.

932 Kusche, J., 2007. Approximate decorrelation and non-isotropic smoothing of
933 time-variable GRACE-type gravity field models. J. Geod 81, 733–749.

934 Kusche, J., Schmidt, R., Petrovic, S., Rietbroek, R., 2009. Decorrelated
935 GRACE time-variable GRACE Gravity Solutions for Science at GFZ and
936 their validation using an Hydrological model. J. Geodesy 83.

937 Le Traon, P., Gauzelin, P., 1997. Response of the Mediterranean mean sea
938 level to atmospheric pressure forcing. J. Geophys. Res. 102, 973–984.

939 Leuliette, E.W., Miller, L., 2009. Closing the sea level budget with
940 altimetry, Argo and GRACE. Geophys. Res. Lett. 36, L04608,
941 doi:10.1029/2008GL036010.

942 Mariotti, A., Struglia, M., Zeng, N., Lau, K., 2002. The Hydrological Cycle
943 in the Mediterranean Region and Implications for the Water Budget of the
944 Mediterranean Sea. J. of Climate 15, 1674–1690.

945 Milly, P., Shmakin, A., 2002. Global modeling of land water and energy
946 balances. Part I: The land dynamics (LaD) model. J. of Hydrometeorology
947 3(3), 283–299.

948 Naeije, M., Scharroo, R., Doornbos, E., Schrama, E., 2008. Global altime-
949 try sea-level service: Glass. Global altimetry sea-level service (GLASS),
950 NUSP-2 report GO 52320 DEO. NIVR/DEOS, Netherlands.

951 Paulson, A., Zhong, S., Wahr, J., 2007. Inference of mantle viscosity from
952 GRACE and relative sea level data. Geophys. J. Int. 171, 497–508.

953 Peltier, W., 2004. Global glacial isostasy and the surface of the ice-age
954 Earth: The ICE-5G (VM2) Model and GRACE. Annual Review of Earth
955 and Planetary Sciences 32, 111.

Peneva, E., Stanev, E., Belokopytov, V., Le Traon, P.Y., 2001. Water transport in the Bosphorus Straits estimated from hydro-meteorological and altimeter data: seasonal to decadal variability. J. Marine Systems 31, 21–33.

Rietbroek, R., Brunnabend, S., Dahle, C., Kusche, J., Flechtner, F., Schröter, J., Timmermann, R., 2009. Changes in total ocean mass derived from GRACE, GPS, and ocean modeling with weekly resolution. J. Geophys. Res. 114, C11004.

Rietbroek, R., Fritsche, M., Brunnabend, S.E., Daras, I., Kusche, J., Schröter, J., Flechtner, F., Dietrich, R., 2011. Global surface mass from a new combination of GRACE, modelled OBP and reprocessed GPS data. J. of Geodynamics doi: 10.1016/j.jog.2011.02.003.

Rixen, M., Beckers, J., Levitus, S., Antonov, J., Boyer, T., Maillard, C., Fichaut, M., Baloupos, E., Iona, S., Dooley, H., Garcia, M., Manca, B., Giorgetti, A., Manzella, G., Mikhailov, N., Pinardi, N., Zavatarelli, M., 2005. The Western Mediterranean deep water: a proxy for climate change . Geophys. Res. Lett 32,L12608, 2949–2952.

Rodell, M., Famiglietti, J., Chen, J., Seneviratne, S., Viterbo, P., S., H., C.R., W., 2004. Basin scale estimates of evapotranspiration using GRACE and other observations. Geophys. Res. Lett. 31 L20504, doi:10.1029/2004GL020873.

Spada, G., Stocchi, P., 2007. SELEN: A Fortran 90 Program for solving the sea-level equation. Computer and Geosciences 33, 538–562.

Stanev, E., Bowman, J., Elissaveta, L., Peneva, E., Staneva, J., 2003. Control of Black Sea intermediate water mass formation by dynamics and topography: Comparison of numerical simulations, surveys and satellite data. J. Marine Systems 61, 59–99.

Stanev, E., Le Traon, P., Peneva, E., 2000. Sea level variations and their dependency on meteorological and hydrological forcing: Analysis of altimeter and surface data for the Black Sea. J. Geophys. Res. 105, 17,203–17,216.

Stanev, E., Peneva, E., 2002. Regional sea level response to global climatic change: Black Sea examples. Global and Planetary Changes 32, 33–47.

Stanev, E., Staneva, J., Bullister, L., Murray, J., 2004. Ventilation of the Black Sea pycnocline: Parameterization of convection, numerical simulations and validations against observed chlorofluorocarbon data. Deep Sea Res. 51(12), 2137–2169.

Swenson, S., Wahr, J., 2002. Methods for inferring regional surface-mass anomalies from Gravity Recovery and Climate Experiment (GRACE) measurements of time-variable gravity. J. Geophys. Res. 107, 3–1.

Swenson, S., Wahr, J., 2006. Post-processing removal of correlated errors in GRACE data. Geophys. Res. Lett. 33, L08402.

Swenson, S., Wahr, J., 2007. Multi-sensor analysis of water storage variations of the Caspian Sea. Geophys. Res. Lett. 34, L1640.

Tapley, B.D., Bettadpur, S., Ries, J.C., Thompson, P.F., Watkins, M.M., 2004. GRACE Measurements of Mass Variability in the Earth System. Science 305, 503–506.

1002 Tonani, M., Pinardi, N., Dobricic, S., Pujol, I., Fratianni, C., 2008. A high-
1003 resolution free-surface model of the Mediterranean Sea. Ocean Sci. 4, 1–14.

1004 Velicogna, I., Wahr, J., 2006. Measurements of Time-Variable Gravity Show
1005 Mass Loss in Antarctica. Science Express .

1006 Wahr, J., Molenaar, M., Bryan, F., 1998. Time variability of the Earth's
1007 gravity field: Hydrological and oceanic effects and their possible detection
1008 using GRACE. J. Geophys. Res. 103, 30205–30230.

1009 Willis, J.K., Chambers, D., Nerem, R., 2008. Assessing the globally averaged
1010 sea level budgt on seasonal to interannal timescales. J. Geophys. Res. 113,
1011 C06015, doi:10.1029/2007JC004517.

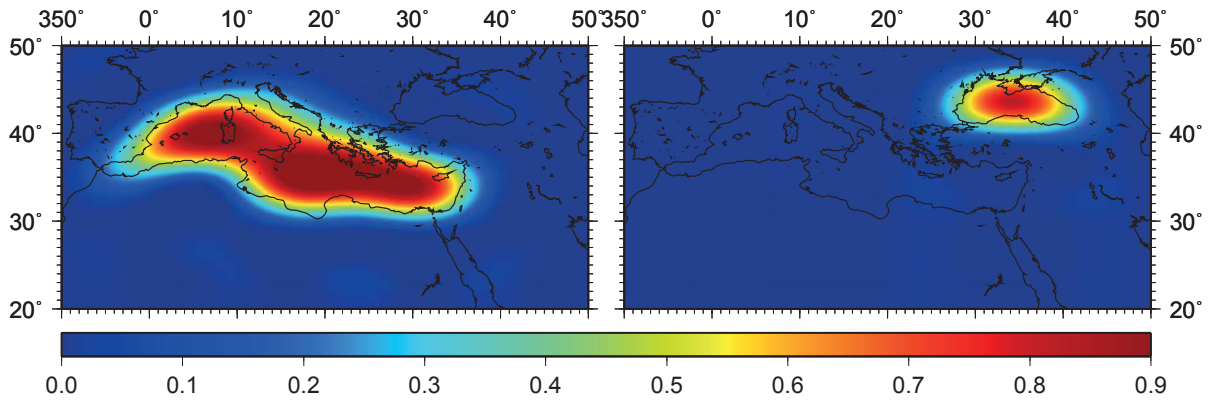

Figure 1: Anisotropically filtered (DDK3) basin kernels of the Mediterranean and Black Sea (Sea of Azov is included).

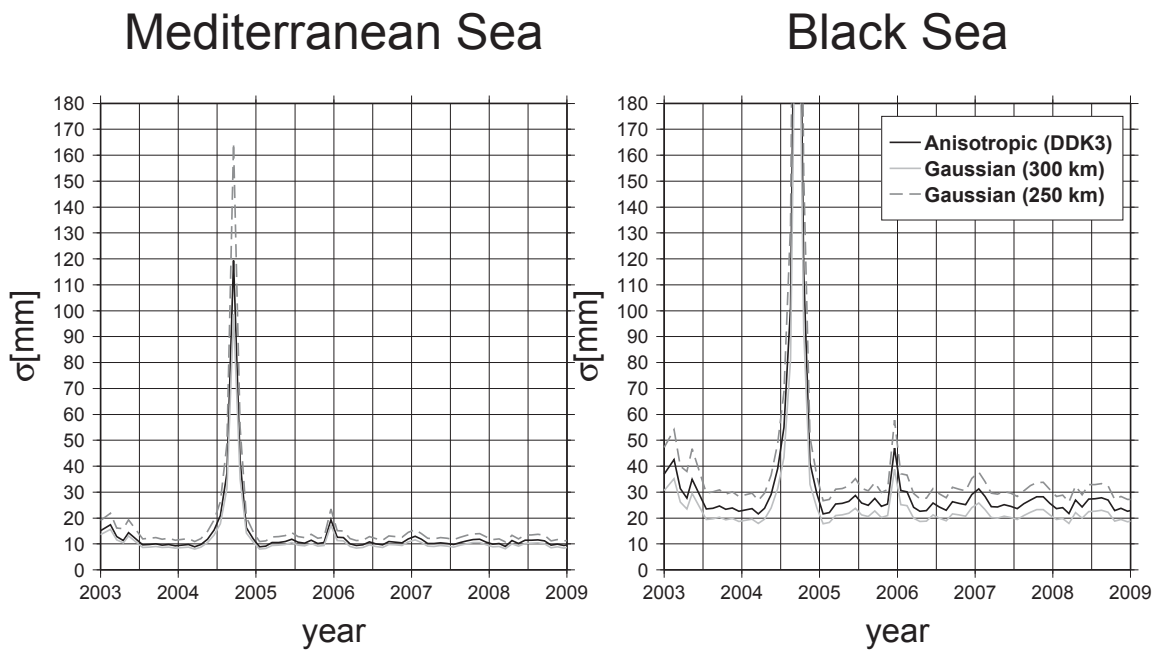

Figure 2: Estimated error of GRACE monthly basin averages derived from GRACE calibrated errors. Peak errors during 2004 will in practice be smaller (but biased) since those solutions are replaced by the constrained solutions.

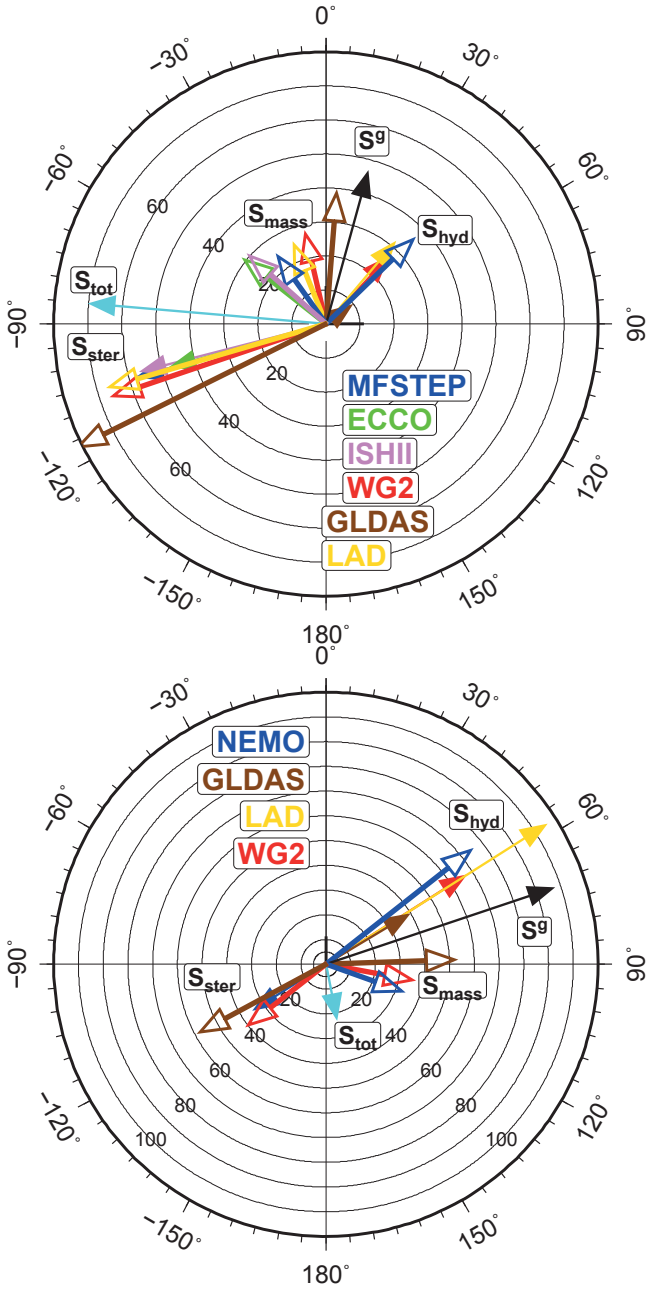

Figure 3: Annual amplitude and phase in Mediterranean Sea (top) and in Black Sea (bottom) of mass-induced sea level change (S_{mass}) and of observed and inferred estimates of steric correction (S_{ster}) and continental hydrological leakage (S_{hyd}) for selected land hydrology and ocean models. The parameters derived from GRACE- and altimetric sea level observations (S^g and S_{tot}) are kept fixed. Three land hydrology models are used in each basins. Three ocean models in the Mediterranean Sea and one in the Black Sea are used. Full/empty markers indicate observed/inferred quantities.

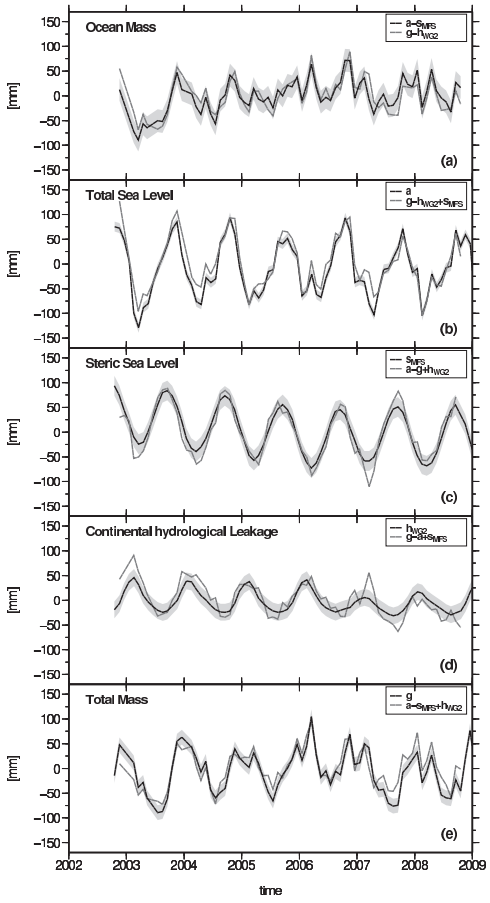

Figure 4: Mediterranean Sea: Basin average of water mass variation expressed in equivalent water height (a), total sea level (b) and its steric component (c), continental hydrological leakage correction (d) and mass change including hydrological leakage (e). In (a): water mass change is from steric-corrected altimetry (black) and from hydrology- corrected GRACE gravity solutions (gray), where g is the rescaled mass change computed as GRACE-load+GAD-GIA as described in Section 2.1. In b-e: observed (b,e) and modeled (c,d) quantities are black, while inferred estimates, computed by adding or subtracting the other three observational/modeled estimates as in Eq. 7, are gray. Error bounds correspond to the RMS differences, unknown systematic errors may remain (Table 7).

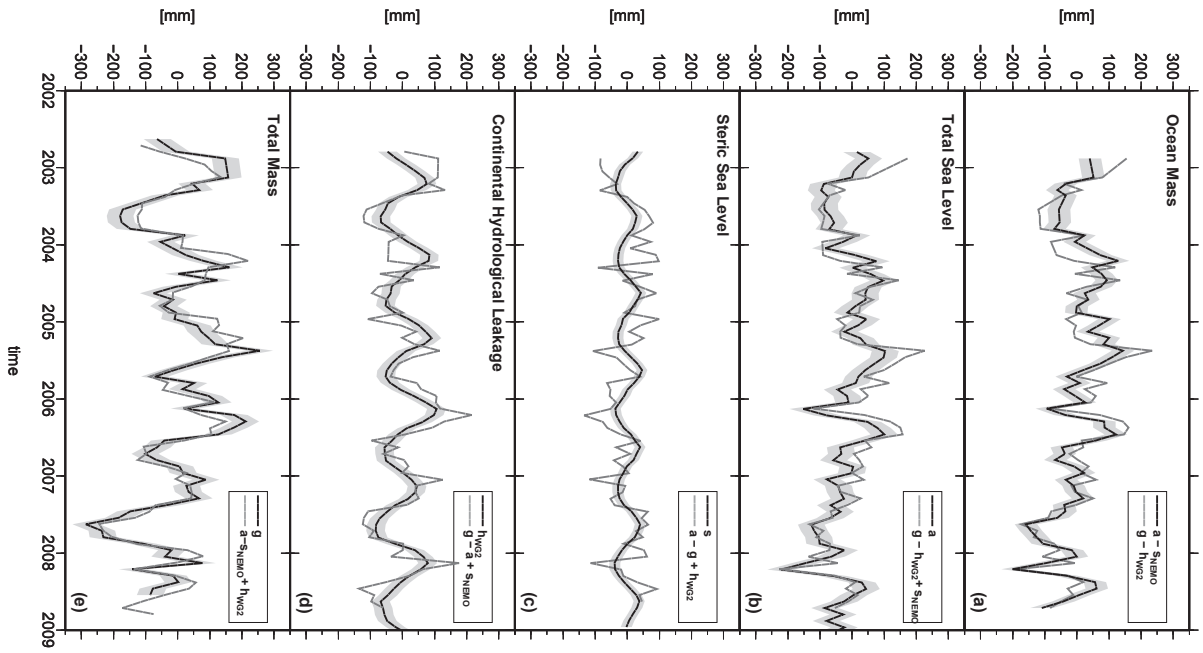

Figure 5: As in Figure 4, but for the Black Sea.

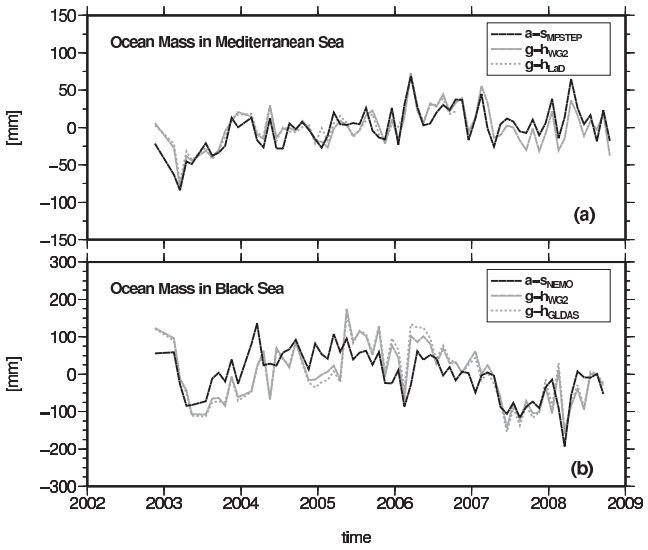

Figure 6: Inter-annual basin average in Mediterranean Sea (a) and in Black Sea (b) of the mass induced sea level (annual cycle removed) from filtered steric-corrected altimetry (black) and from hydrology-corrected GRACE (grey). Steric corrections come from MF-STEP in (a) and from NEMO in (b), continental hydrological leakage corrections come from WaterGAP2 (line) and LAD (dots) in (a) and from WaterGAP2 (line) and GLDAS (dots) in (b).

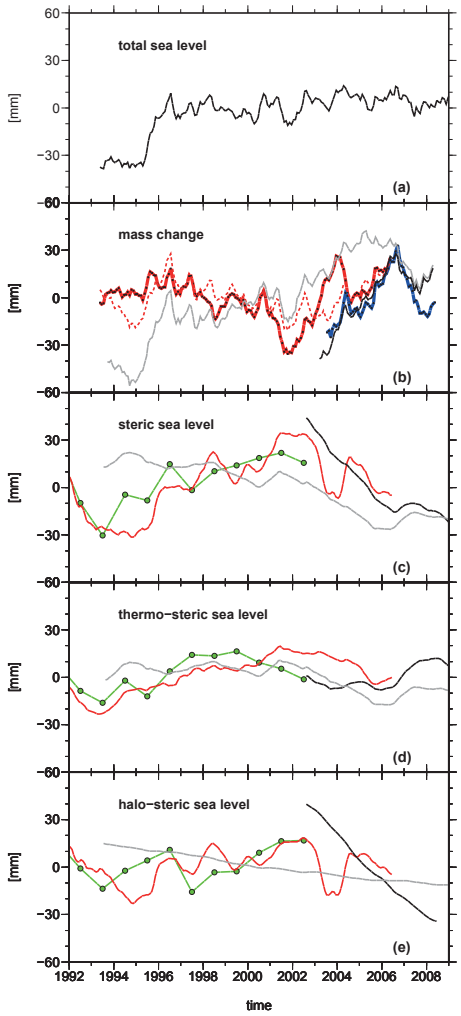

Figure 7: Basin averages in the Mediterranean Sea of (a) total sea level from multi-mission satellite altimetry, (b) mass change from GRACE (black) and from steric-corrected altimetry with steric correction from MFSTEP (blue), ECCO (gray) and Ishii climatology v6.7 (red) and with thermo-steric correction from Ishii climatology v6.7 (dashed), (c) steric, (d) halo-steric and (e) thermo-steric components of sea level with color notation as above. A moving average of 12 months has been applied to the monthly values. Annual values from MEDAR are also shown (green).

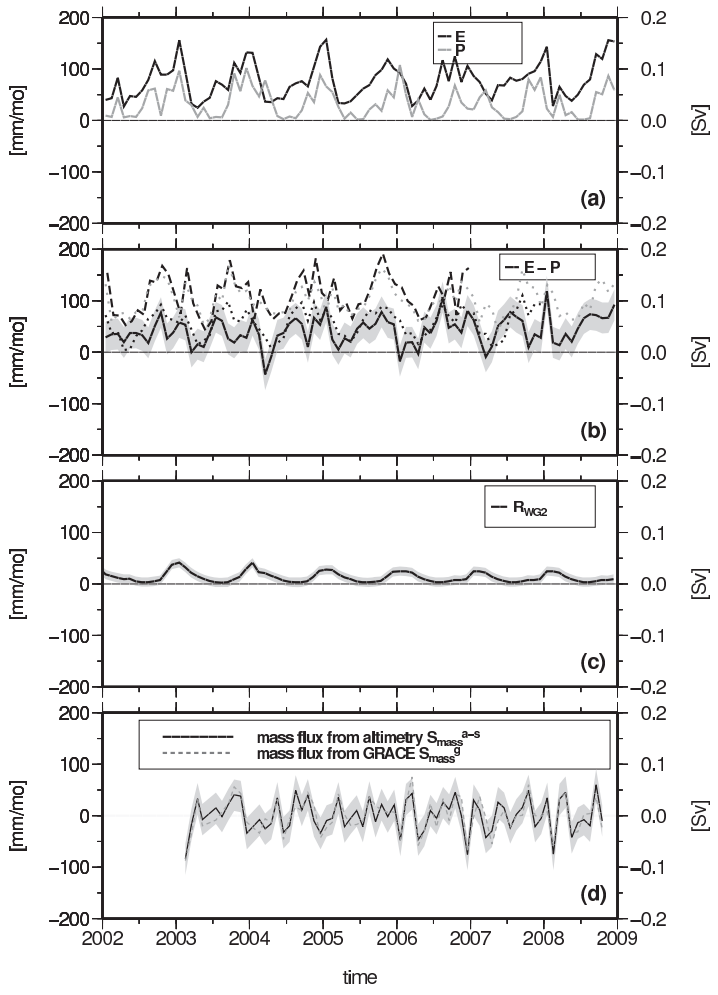

Figure 8: Mediterranean water mass fluxes (as uniform basin changes and volume flow): (a) Evaporation (black) and Precipitation (grey), (b) Precipitation minus Evaporation, (c) river runoff, (d) total mass flux derived from GRACE ($\dot{\hat{S}}^{g-h}_{mass}$, gray) and from altimetry ($\dot{S}^{a-s}_{mass}$, black). In (b) $E - P$ is from ECMWF (solid line), OAFLUX-CPCP (black dots), ERA (gray dots) and DFS4 (black dashed line). Error bounds correspond to RMS differences, unknown systematic errors may remain (see Tab. 7).

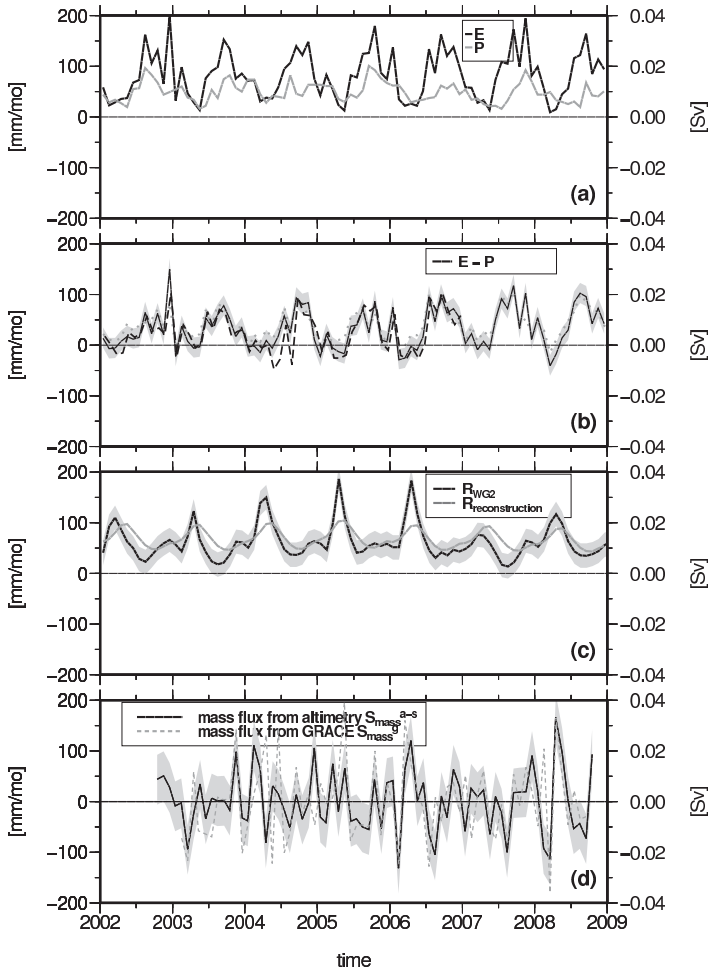

Figure 9: As in Figure 8, but for the Black Sea mass fluxes. In (b) $E-P$ is from ECMWF (full line), ERA (grey dots) and DFS4 (dark dashed line). In (d) the series depict $\dot{\hat{S}}^{g-h}_{mass}$ and $\dot{S}^{a-s}_{mass}$. Error bounds (light gray) correspond to RMS differences, unknown systematic errors may remain (see Tab. 7).

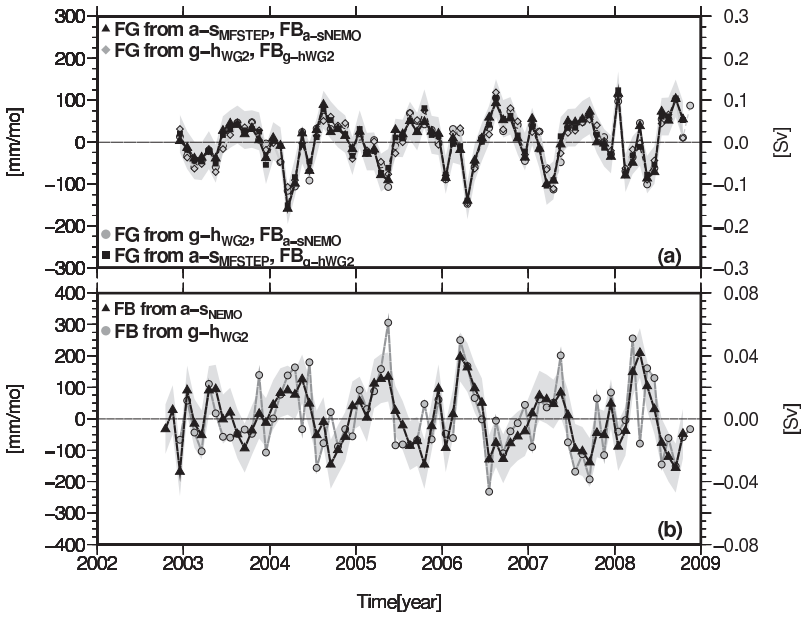

Figure 10: Monthly estimates of the strait flow anomalies at Gibraltar, FG, (a) and at the Bosphorus strait, FB, (b) both as uniform layer changes in the Mediterranean Sea and in the Black Sea (mm/mo) and as volume transport (Sv). FB is derived from both GRACE-based (circle) and altimetry-based mass variation estimates (triangle). FG is derived from both GRACE-based/only (diamond) and altimetry-based/only (triangle) mass estimates in both basins and from mixed GRACE-based and altimetry-based estimates (circle and square). Error bounds (light gray) correspond to the altimetry-based/only estimates (Table 7).

Table 1: Scaling factors derived from smoothed and unsmoothed basin kernels up to a maximum degree (truncation at degree $50, 70, 100$ (d50, d70, d100)) and from direct comparison of unfiltered and filtered mass change from steric-corrected altimetry ($\frac{S^{a-s}_{mass}}{\widetilde{S}^{a-s}_{mass}}$)

	Mediterranean Sea				Black Sea			
	d100	d70	d50	$(\frac{S^{a-s}_{mass}}{\widetilde{S}^{a-s}_{mass}})$	d100	d70	d50	$(\frac{S^{a-s}_{mass}}{\widetilde{S}^{a-s}_{mass}})$
unfiltered	1.17	1.25	1.31	1.7	1.19	1.3	1.47	1.0
Gauss R300	1.61	1.61	1.61	1.5	2.22	2.22	2.22	1.9
DDK3	1.39	1.39	1.39	1.4	1.62	1.62	1.62	1.7

Table 2: Comparison of mass induced sea level from GRACE, $\hat{S}^{g-h}_{mass}$, with the altimetry-derived estimate, S^{a-s}_{mass}, for a variety of hydrological and steric corrections. The table shows the agreement of the series in terms of correlation and RMS difference of the monthly and the inter-annual series, denoted by the subscript $_{mon}$ and $_{ia}$ respectively. In addition, the difference of the (semi-) annual amplitudes and phases are provided. The interval of analysis is from August 2002 to July 2008. Ishii and LAD/Fraser are only available from August 2002 to July 2006 (corresponding fields are denoted by an $*$).

s	h	$corr_{mon}$	RMS_{mon} (mm)	ΔA (mm)	$\Delta\varphi_A$ (days)	ΔA_{SA} (mm)	$\Delta\varphi_{SA}$ (days)	$corr_{ia}$	RMS_{ia} (mm)
MFSTEP	WG2	0.86	37	3	23	6	4	0.85	15
ECCO	WG2	0.78	67	3	30	7	4	0.84	13
Ishii*	WG2	0.75	41	3	32	3	7	0.69	21
MFSTEP	GLDAS	0.66	32	14	41	0	4	0.66	21
MFSTEP	LAD*	0.91	25	1	14	1	6	0.89	12
NEMO	WG2	0.71	120	3	9	12	16	0.68	55
NEMO	GLDAS	0.69	66	20	31	6	4	0.64	60
NEMO	LAD*	0.51	81	12	69	13	123	0.50	59

Table 3: Mediterranean Sea: Annual (A) and semi-annual (SA) amplitude and phase and trend for various sea level components. The component type is indicated by the subscript ($_{tot}$: total sea level, $_{ster}$: steric sea level, $_{mass}$: mass induced sea level $_{hyd}$: hydrological leakage). Filtered fields, which have been scaled to account for signal attenuation, are denoted by a hat. The superscript, indicate the used datasets (^{a}: altimetry, ^{s}: steric modelling, ^{g}: GRACE, ^{h}: hydrological modelling), which are in some cases augmented with the model name/dataset. The interval of analysis is from August 2002 to July 2008. Ishii and LAD/Fraser are available only from August 2002 to July 2006 (the corresponding fields are denoted by an $*$).

Field	A Amp (mm)	A Phase (days)	SA Amp (mm)	SA Phase (days)	Trend ($\frac{mm}{yr}$)
$S^{a_{J1}}_{tot}$	70±2	278±4	13±1	121±1	0.8±1.3
S^{g-h+s}_{tot}=$\hat{S}^{g-h}_{mass} + S^{s}_{ster}$	64±5	282±1	19±3	121±1	-4.0±2.9
$S^{h_{WG2}}_{hyd}$	27±3	44±6	2±3	34±3	-1.0±0.6
$S^{*h_{LaD}}_{hyd}$	32±4	41±8	2±4	35±4	-1.0±0.6
$S^{h_{GLDAS}}_{hyd}$	10±4	53±6	0.3±4	172±4	-0.7±0.6
S^{g-a+s}_{hyd} =$\hat{S}^{g}$ - $S^{a_{J1}}_{tot}$ + $S^{s_{MFSTEP}}_{ster}$	34±4	47±7	1±5	1±5	-8.7±2.1
$\hat{S}^{g}$	46±4	16±3	15±5	125±5	2.1±2.5
$S^{s_{MFSTEP}}_{ster}$	58±4	258±4	0.4±4	86±4	-10.1±0.6
$S^{s_{ECCO}}_{ster}$	48±4	258±2	0.8±4	141±4	-3.1±0.4
$S^{*s_{Ishii}}_{ster}$	57±4	259±2	2±4	12±4	-5.8±0.4
S^{a-g+h}_{ster} = $S^{a_{J1}}_{tot}$ - $\hat{S}^{g-h_{WG2}}_{mass}$	66±4	255±3	6±3	31±3	-5.3±1.1
S^{a-g+h}_{ster} = $S^{a_{J1}}_{tot}$ - $\hat{S}^{g-h_{GLDAS}}_{mass}$	80±4	249±3	1±3	34±3	-3.1±1.2
S^{*a-g+h}_{ster} = $S^{a_{J1}}_{tot}$ - $\hat{S}^{g-h_{LaD}}_{mass}$	66±4	257±3	2±3	75±3	-10.4±1.2
$S^{a-s}_{mass} = S^{a_{J1}}_{tot} - S^{s_{ECCO}}_{ster}$	30±5	312±5	12±3	119±3	2.9±1.6
$S^{a-s}_{mass} = S^{a_{J1}}_{tot} - S^{s_{MFSTEP}}_{ster}$	24±5	329±6	13±3	119±3	8.3±1.6
$S^{*a-s}_{mass} = S^{a_{J1}}_{tot} - S^{s_{MFSTEP}}_{ster}$	25±5	327±6	14±3	118±3	19.2±1.6
$S^{*a-s}_{mass} = S^{a_{J1}}_{tot} - S^{*s_{Ishii}}_{ster}$	30±5	316±5	16±5	116±5	6.8±1.8
$\hat{S}^{g-h}_{mass} = \hat{S}^{g-h_{WG2}}_{mass}$	27±5	352±9	19±5	123±5	5.3±1.9
$\hat{S}^{g-h}_{mass} = \hat{S}^{g-h_{GLDAS}}_{mass}$	38±6	5±6	13±5	123±5	2.8±1.9
$\hat{S}^{*g-h}_{mass} = \hat{S}^{g-h_{LaD}}_{mass}$	25±6	343±6	15±5	124±5	14.9±2.9

Table 4: As in Tab. 3 but for the Black Sea.

Field	A Amp (mm)	A Phase (days)	SA Amp (mm)	SA Phase (days)	Trend ($\frac{mm}{yr}$)
$S_{tot}^{a_{J1}}$	23±4	171±5	28±4	155±3	-4.3±1.9
S_{tot}^{g-h+s}=$\hat{S}_{mass}^{g-h} + S_{ster}^{s}$	32±7	184±5	41±5	148±1	-11.2±4.9
$S_{hyd}^{h_{WG2}}$	68±7	58±6	10±5	50±5	-0.3±0.6
$S_{hyd}^{*h_{WLaD}}$	106±10	58±8	8±4	73±4	1.3±0.6
$S_{hyd}^{h_{GLDAS}}$	40±5	60±6	2.3±4	70±4	-3.2±0.6
S_{hyd}^{g-a+s} =$\hat{S}^{g}$ - $S_{tot}^{a_{J1}}$ + $S_{ster}^{s_{NEMO}}$	74±4	53±7	22±5	111±5	-2.5±1.1
$\hat{S}^{g}$	97±10	72±3	38±5	150±5	-19.4±2.5
$S_{ster}^{s_{NEMO}}$	35±4	241±4	3.5±4	38±4	-0.3±0.6
$S_{ster}^{s_{WOA05}}$	29±4	238±2	0.8±4	41±4	
S_{ster}^{a-g+h} = $S_{tot}^{a_{J1}}$ - $\hat{S}_{mass}^{g-h_{WG2}}$	40±4	235±3	19±3	32±3	0.2±1.1
S_{ster}^{a-g+h} = $S_{tot}^{a_{J1}}$ - $\hat{S}_{mass}^{g-h_{GLDAS}}$	57±4	245±3	13±3	12±3	-6.3±1.2
$S_{mass}^{a-s} = S_{tot}^{a_{J1}} - S_{ster}^{s_{NEMO}}$	32±5	111±10	33±3	163±10	-12.2±5.6
$S_{mass}^{*a-s} = S_{tot}^{a_{J1}} - S_{ster}^{s_{ECCO}}$	34±5	118±10	26±3	166±10	11.2±5.6
$\hat{S}_{mass}^{g-h} = \hat{S}_{mass}^{g-h_{WG2}}$	35±5	102±10	45±4	147±10	-12.2±1.9
$\hat{S}_{mass}^{g-h} = \hat{S}_{mass}^{g-h_{GLDAS}}$	52±6	89±10	36±5	151±5	-8.8±1.9
$\hat{S}_{mass}^{*g-h} = \hat{S}_{mass}^{g-h_{LaD}}$	44±6	180±10	46±5	30±5	30±1.9

Table 5: Annual (A) and semi-annual (SA) amplitude and phase and the trend of water fluxes of the Mediterranean Sea. The time interval is August 2002 - July 2008. The Bosphorus and the Gibraltar strait flows, expressed in the rate of change of an uniform layer in the Mediterranean Sea are indicated by the subscripts $_{FB}$ and $_{FG}$ respectively.

	A Amp ($\frac{mm}{mon}$)	A Phase (days)	SA Amp ($\frac{mm}{mon}$)	SA Phase (days)	Trend (($\frac{mm}{mon}$)/year)
$\dot{S}^{a-s}_{mass}$	13±7	252±16	13±7	92±10	0.8±0.3
$\dot{\hat{S}}^{g-h}_{mass}$	16±5	271±16	18±8	94±10	1.5±0.3
$\dot{S}_{E-P}$	19±7	266±16	17±7	9±10	2.5±0.3
$\dot{S}_{R}$	12±4	5±22	5±4	117±10	0.5±0.3
$\dot{S}^{a-s}_{FB}$	16±4	91±6	6±5	130±5	-0.8±0.4
$\dot{S}^{g-h}_{FB}$	13±4	80±5	9±5	117±10	-0.1±0.4
$\dot{S}^{a-s}_{FG}$ (from $\dot{S}^{a-s}_{FB}$)	53±10	264±5	19±8	31±10	2.2±0.8
$\dot{S}^{a-s}_{FG}$ (from $\dot{S}^{g-h}_{FB}$)	51±11	261±5	42±5	27±7	2.1±0.8
$\dot{S}^{g-h}_{FG}$ (from $\dot{S}^{a-s}_{FB}$)	55±11	274±5	19±8	48±8	3.6±0.8
$\dot{S}^{g-h}_{FG}$ (from $\dot{S}^{g-h}_{FB}$)	52±11	271±5	21±5	41±8	3.4±0.8

Table 6: As in Tab. 5, but for the Black Sea. All values are expressed as the rate of change of an uniform layer in the Black Sea.

	A Amp $(\frac{mm}{mon})$	A Phase (days)	SA Amp $(\frac{mm}{mon})$	SA Phase (days)	Trend $((\frac{mm}{mon})$/year)
$\dot{S}^{a-s}_{mass}$	16±2	32±16	34±2	133±10	-0.1±0.3
$\dot{\hat{S}}^{g-h}_{mass}$	11±7	44±16	41±7	113±10	3.8±0.3
$\dot{S}_{E-P}$	40±5	264±16	7±5	17±8	2.1±0.3
$\dot{S}_R$	22±6	116±12	7±6	140±10	-0.9±0.3
$\dot{S}^{a-s}_{FB}$	94±14	91±6	34±10	130± 10	-2.0±0.8
$\dot{S}^{g-h}_{FB}$	81±18	80±5	58±10	117± 10	-0.1±0.9

Table 7: Monthly errors σ_m (mm) and propagated errors of annual amplitude σ_A ($\frac{2}{\sqrt{N}}\sigma_m$) ($mm$, $\frac{mm}{mon}$) in Mediterranean (left) and Black Sea (right), for the time interval from August 2002 to July 2008 (N=72). The estimate is obtained from the root mean square of differences (RMS) or from error propagation (EP).

	Med Sea			Black Sea		
	σ_m	σ_A	Method	σ_m	σ_A	Method
S^a_{tot}	10	2	RMS	30	8	RMS
$S^{g-h+s}_{tot} = \hat{S}^{g-h}_{mass} + S^s_{ster}$	30	7	EP	54	13	EP
S^h_{hyd}	17	5	RMS	29	8	RMS
$S^{g-a+s)}_{hyd} = \hat{S}^g$ - $S^a_{tot} + S^s_{ster}$	27	6	EP	54	13	EP
S^s_{ster}	20	5	RMS	17	4	RMS
$S^{a-g+h}_{ster} = S^a_{tot}$ - $\hat{S}^{g-h}_{mass}$	24	6	EP	27	10	EP
S^g	15	4	EP	42	10	EP
S^{a-s}_{mass}	22	5	EP	35	8	EP
S^{g-h}_{mass}	23	6	EP	51	12	EP
$\dot{S}^{a-s}_{mass}$	31	7	EP	49	12	EP
$\dot{S}^{g-h}_{mass}$	33	8	EP	72	17	EP
$\dot{S}_{E-P}$	30	7	RMS	20	5	RMS
$\dot{S}_R$	9	2	RMS	24	6	RMS
$\dot{S}^{a-s}_{FB}$	10	2	EP	58	14	EP
$\dot{S}^{g-h}_{FB}$	13	3	EP	78	18	EP
$\dot{S}^{a-s}_{FG}$ (from $\dot{S}^{a-s}_{FB}$)	44	10	EP			
$\dot{S}^{g-h}_{FG}$ (from $\dot{S}^{g-h}_{FB}$)	45	11	EP			